Supplementary methods

Microarray gene expression profiling

Full description of the methods and results for each experiment are available at http://www.ebi.ac.uk/microarray-as/aer/#ae-main[0] (accession numbers E-NCMF-21 and E-NCMF-27 for rat and human data, respectively). The Agilent human probes that were significantly up- or down-regulated by both Fra-1 shRNAs ($p<1.10^{-6}$) were selected and mapped to the corresponding Affymetrix U133A probes using Martview from BioMart (http://www.biomart.org/index.html). We selected a single Affymetrix HGU-133A probe for each Entrez ID based on the Affymetrix algorithm probe extension, favoring '_at' over '_x_at' over '_s_at'. Expression of remaining duplicate probes were averaged, resulting in a 1234 probe set.

Classifier generation and analysis

We collected six publicly available datasets based on Human Genome HGU-133A Affymetrix arrays from NCBI's Gene Expression Omnibus (GEO, http://www.ncbi.nlm.nih.gov/geo/) with the following identifiers; GSE6532 (1), GSE3494 (2), GSE1456 (3), GSE7390 (4) and GSE5327 (5). The Chin et al. (6) data set was downloaded from ArrayExpress (http://www.ebi.ac.uk/, identifier E-TABM-158).

To ensure comparability between the different datasets, they were all subjected to the same pre-processing procedure. Microarray quality-control assessment was carried out using the R AffyPLM package (Bioconductor, http://www.bioconductor.org). We applied the Relative Log Expression (RLE) and Normalized Unscaled Standard Errors (NUSE) tests. Chip pseudo-images were produced to assess artefacts, and 1 to 5% of the arrays of the

datasets did not pass the quality control tests. Selected arrays were normalized according to a 3-step procedure using the RMA expression measure algorithm (http://www.bioconductor.org): RMA background correction convolution, median centering of each gene across arrays separately for each data set and quantile normalization of all arrays. Out of the 947 unique collected microarray samples of sufficient quality, 509 had Distant Metastasis Free Survival (DMFS) data available. We employed these samples as training set, and will denote this sets as the 'Affymetrix training set'.

From the experimental Fra-1 signature 1234 unique probes, probes were extracted that exhibited a significant P-value ($P<0.05$, log-rank test) on the Affymetrix training set. This resulted in a subset of 183 probes. Next, we employed the Affymetrix training set to define a nearest centroid classifier for these 183 probes. The 'poor prognosis' centroid was derived from the samples with a metastatic event before 60 months of follow-up. The 'good prognosis' centroid was derived from the samples with no metastatic event and a follow-up longer than 60 months.

For the analysis of publicly available datasets and comparison with other signatures, the genes or probe-sets in every signature were classified as UP if they were associated with cancer or poor prognosis in the definition of the signature and classified as DOWN otherwise. For a given signature S and dataset D, the genes or probe-sets of S were mapped to the genes or probe-sets of D. If a single gene or probe-set in S mapped to multiple genes or probe-sets of D, then the gene or probe-set of D with the most variance across D was used. For each signature S and patient W in D, we defined the signature activation to be the mean of the expression levels in W of the UP genes of S minus the mean of the expression levels in W of the DOWN genes of S. To form Figure 3B, for each signature and dataset, a Cox proportional hazards model was fit to the signature activation and the time to distant metastasis (if available) or relapse.

Fig. 3*C* and Fig. S10 were made as follows. Signature activations were computed as described above. Then, for each subtype (e.g., ER pos / Her2 neg), for each dataset the patients belonging to the subtype were classified as signature-high if their signature activations were above the median signature activation for patients in that dataset and subtype and as signature-low otherwise. Then a log-rank analysis was performed comparing all the signature-high patients belonging to the subtype in all the datasets with all the signature-low patients belonging to the subtype in all the datasets. The datasets were combined in this way to achieve sufficient power. We had ER and Her2 subtype information for only a subset of the datasets. The survival data used for the log-rank and Cox proportional hazards analysis was time to distant metastasis (if available) or relapse.

Antibodies

BDNF (N-20), Fra-1 (R-20), and Trk (C-14) antibodies were from Santa Cruz, α-catenin (610193), β-catenin (14), γ-catenin (610253) and E-cadherin (610181) antibodies were from Becton Dickinson. α-tubulin antibody (DM1A) was from Sigma. Vimentin antibody (SP20) was from Thermo Scientific. GFP antibody (6556) was from Abcam. Phospho-ERK antibody (9106) was from Cell Signaling.

Immunofluorescence

Immunofluorescence experiments were performed as previously described (47). Fra-1 antibody (1:200), E-cadherin antibody (1:200), Alexa568-coupled phalloidin (A12380, Invitrogen; 1:200), α-tubulin antibody (T9026, Sigma; 1:3000) and an AlexaFluor647-coupled goat-anti-mouse secondary antibody (A21237, Invitrogen; 1:500) were used.

Immunohistochemistry

Histological sections and haematoxylin-eosin staining were performed using standard procedures. Paraffin sections were deparaffinized, rehydrated, pretreated in 0.1 mM sodium citrate pH 6.0, washed and incubated with peroxide. The tissue was incubated with primary antibodies for Fra-1 (1:200) or Vimentin (1:200). Secondary antibody was PowerVision + (DPVB + 999HRP; ImmunoLogic). Peroxidase activity was detected with Liquid DAB (K3468; DAKO).

Gel shift experiments

Gel shift experiments were performed as previously described (7). The sense strand of the AP-1 probe used had the following sequence: 5'-GGTTCGCTTGATGAGTCAGCCGGAA-3'. For supershift experiments, the nuclear extracts were pre-incubated with 2 μg of anti-Fra-1 antibody for 30 min.

Real-Time RT-PCR

RT-PCR experiments were performed as previously described (8). The sequence of the primer sets used are described in Table S2. Rat Fra-1 mRNA levels were normalized using rat HPRT1 mRNA levels and human Adenosine receptors mRNA levels were normalized using human beta-Actin mRNA levels.

Chromatin immunoprecipitation

ChIP experiments were performed as previously described (9). Briefly, approximately 2 x 10^8 LM2 cells per condition were crosslinked with 1% formaldehyde. Cells were harvested, lysed and chromatin was fragmented by sonication in a Bioruptor (Diagenode), in a 30 min cycle of 30s ON, 30s OFF at 4 °C and maximum level. In parallel, 100 μl of magnetic beads (Dynabeads, Invitrogen) were prepared by washing 3x with 0.5% BSA in PBS and incubated

o/n with 20 µg Fra-1 antibody (N-17, sc183x, Santa Cruz) or 20 µg rabbit IgG as a control. 50 µl of lysate was kept as whole cell extract and the remainder was added to the antibody/magnetic bead mix and incubated o/n. Afterwards beads were washed 12x with RIPA buffer and finally once more with TBS. Samples were eluted from the beads and reverse-crosslinking was performed at 65 °C for 6 h.

DNA was extracted via phenol-chloroform-isoamylalcohol phases separated with 2.0 ml Phase Lock Gel Light tubes (5Prime) according to the manufacturers protocol. DNA was pelleted, washed and dissolved in TE buffer.

Real-time PCR primer sets (Supplementary Table 3) were designed based on bioinformatic data from publicly available ChIP-seq datasets (genome.ucsc.edu\ENCODE). Binding peaks for c-Fos and/or Jun, which were considered putative Fra-1 binding sites, were identified in the *ADORA2B* gene on multiple places and 5 were chosen due to conservation over a range of cell types (Fig. S12*C*). Negative control primer sets were designed for 2 random regions that did not show a binding peak. Real-time PCR was performed on a StepOne Plus with standard SYBR Green mix (Life Technologies). Data was normalized to primer efficiency and negative control 1.

Quantification of pulmonary metastasis

Mice were sacrificed using CO2 asphyxiation and the lungs were subsequently removed and dissected. Lungs were fixed in an Ethanol/Acetic acid/Formol saline fixative (EAF) and examined under a stereoscope. Macroscopic pulmonary metastases were identified as aberrant white masses on the surface of the lungs. For histological assessment of metastases, 8 sections from independent positions in the lungs were stained with hemoatoxylin-eosin (H&E) and the total number of metastases in these sections was determined. Alternatively, lungs were fixed in formaldehyde and imaged within 2 hours by fluorescence microscopy for quantification of

the fluorescence emitted by GFP-labeled LM2 cells. Images were taken with the same intensities and exposure times, and the mean fluorescence intensity per surface area occupied by tumor cells was quantified using ImageJ software (http://rsb.info.nih.gov/ij/download.html) with the MBF plug-in bundle (http://www.macbiophotonics.ca/downloads.htm).

Retro- and lentiviral transduction

Retroviral transductions were performed as described (http://www.stanford.edu/group/nolan/retroviral_systems/phx.html). RIE-1 and RK3E cells were retrovirally transduced with murine TrkB and BDNF expression constructs as previously described (10), except that the TrkB cDNA was subcloned into pMSCV-blasticidin. Retroviral silencing of Fra-1 in RK3E cells was performed using the pRS-puro vector with the following targeting sequences: *sh*-Fra-1(1) (TAACTAGCCTAGAACACTA) and *sh*-Fra-1(2) (GAAGTTCCACCTTGTGCCA). As negative control, pRS-puro without insert was used. Lentiviral transductions were performed as described previously (11). Luciferase was subcloned into lentiviral vector HIV-CS-CG. Silencing of Fra-1 in LM2 and MDA-MB-231 cells was performed using the following targeting sequences: *sh*-Fra-1(1) (GTAGATCCTTAGAGGTCCT) and *sh*-Fra-1(2) (GGCCTGTGCTTGAACCTGA). As negative control, vector without insert was used. Cells were infected once ($2x10^6$ cells with $1.5x10^7$ viral particles) and GFP-positive cells were selected by fluorescence activated cell sorting (FACS). Silencing of ADORA2B in LM2 cells was performed using pLKO.1 vectors from the TRC library (Sigma). sh-ADORA2B(1): TRCN0000065334, sh-ADORA2B(2): TRCN0000065335,, sh-ADORA2B(3): TRCN0000065336 and sh-ADORA2B(4): TRCN0000065337. As a negative control, vector without insert was used. Cells were infected once and then selected for puromycin resistance.

TRCN0000065337. As a negative control, vector without insert was used. Cells were infected once and then selected for puromycin resistance.

Supplementary Table 1: Fra1 classifier

Affymetrix Probe ID	Entrez ID	HGNC Symbol	Poor Prognostic Centroid	Good Prognostic Centroid	Gene Description
200034_s_at	6128	RPL6	-0.08	0.03	ribosomal protein L6 /// ribosomal protein L6
200620_at	9528	TMEM59	-0.14	0.03	transmembrane protein 59
200640_at	7534	YWHAZ	0.14	-0.08	tyrosine 3-monooxygenase/tryptophan 5-monooxygenase activation protein, zeta polypeptide
200690_at	3313	HSPA9B	0.04	-0.09	heat shock 70kDa protein 9B (mortalin-2)
200756_x_at	813	CALU	0.19	-0.02	calumenin
200760_s_at	10550	ARL6IP5	-0.19	0.06	ADP-ribosylation-like factor 6 interacting protein 5
200761_s_at	10550	ARL6IP5	-0.18	0.06	ADP-ribosylation-like factor 6 interacting protein 5
200827_at	5351	PLOD1	0.14	-0.08	procollagen-lysine 1, 2-oxoglutarate 5-dioxygenase 1
200921_s_at	694	BTG1	-0.17	0.02	B-cell translocation gene 1, anti-proliferative
201114_x_at	5688	PSMA7	0.20	-0.04	proteasome (prosome, macropain) subunit, alpha type, 7
201137_s_at	3115	HLA-DPB1	-0.30	0.04	major histocompatibility complex, class II, DP beta 1
201154_x_at	6124	RPL4	-0.05	0.00	ribosomal protein L4
201172_x_at	8992	ATP6V0E	0.05	-0.03	ATPase, H+ transporting, lysosomal 9kDa, V0 subunit e
201195_s_at	8140	SLC7A5	0.43	-0.10	solute carrier family 7 (cationic amino acid transporter, y+ system), member 5
201242_s_at	481	ATP1B1	-0.19	-0.03	ATPase, Na+/K+ transporting, beta 1 polypeptide
201249_at	6513	SLC2A1	0.03	-0.06	solute carrier family 2 (facilitated glucose transporter), member 1
201254_x_at	6194	RPS6	-0.08	0.03	ribosomal protein S6
201359_at	1315	COPB	0.00	-0.06	coatomer protein complex, subunit beta
201366_at	310	ANXA7	-0.08	-0.05	annexin A7
201506_at	7045	TGFBI	0.21	-0.08	transforming growth factor, beta-induced, 68kDa
201668_x_at	4082	MARCKS	0.11	-0.16	myristoylated alanine-rich protein kinase C substrate
201851_at	6455	SH3GL1	0.01	-0.06	SH3-domain GRB2-like 1
201857_at	51663	ZFR	0.05	-0.02	zinc finger RNA binding protein
201899_s_at	7319	UBE2A	0.05	-0.06	ubiquitin-conjugating enzyme E2A (RAD6 homolog)
201908_at	1857	DVL3	-0.03	-0.18	dishevelled, dsh homolog 3 (Drosophila)
201934_at	80335	PRO2730	-0.14	-0.05	Hypothetical protein PRO2730
201938_at	8099	CDK2AP1	0.11	-0.08	CDK2-associated protein 1
201991_s_at	3799	KIF5B	0.13	-0.06	kinesin family member 5B
202026_at	6392	SDHD	0.00	0.05	succinate dehydrogenase complex, subunit D, integral membrane protein
202088_at	25800	SLC39A6	-0.30	0.11	solute carrier family 39 (zinc transporter), member 6
202094_at	332	BIRC5	0.23	-0.06	baculoviral IAP repeat-containing 5 (survivin)
202107_s_at	4171	MCM2	0.16	-0.05	MCM2 minichromosome maintenance deficient 2, mitotin (S. cerevisiae)
202153_s_at	23636	NUP62	0.04	-0.08	nucleoporin 62kDa
202223_at	3703	ITM1	-0.08	0.02	integral membrane protein 1
202431_s_at	4609	MYC	0.03	-0.05	v-myc myelocytomatosis viral oncogene homolog (avian)
202551_s_at	51232	CRIM1	-0.33	-0.02	cysteine rich transmembrane BMP regulator 1 (chordin-like)
202552_s_at	51232	CRIM1	-0.16	0.06	cysteine rich transmembrane BMP regulator 1 (chordin-like)

202594_at	23484	LEPROTL1	-0.06	0.01	leptin receptor overlapping transcript-like 1
202627_s_at	5054	SERPINE1	0.23	-0.05	serine (or cysteine) proteinase inhibitor, clade E (nexin, plasminogen activator inhibitor type 1), member 1
202628_s_at	5054	SERPINE1	0.19	-0.09	serine (or cysteine) proteinase inhibitor, clade E (nexin, plasminogen activator inhibitor type 1), member 1
202733_at	8974	P4HA2	0.13	-0.15	procollagen-proline, 2-oxoglutarate 4-dioxygenase (proline 4-hydroxylase), alpha polypeptide II
202806_at	1627	DBN1	0.12	-0.08	drebrin 1
202808_at	54838	C10orf26	-0.15	0.00	chromosome 10 open reading frame 26
202833_s_at	5265	SERPINA1	-0.26	0.25	serine (or cysteine) proteinase inhibitor, clade A (alpha-1 antiproteinase, antitrypsin), member 1
202998_s_at	4017	LOXL2	0.23	-0.08	lysyl oxidase-like 2
203045_at	4814	NINJ1	-0.19	-0.02	ninjurin 1
203358_s_at	2146	EZH2	0.31	0.00	enhancer of zeste homolog 2 (Drosophila)
203418_at	890	CCNA2	0.40	0.05	cyclin A2
203590_at	1783	DNCLI2	0.01	-0.11	dynein, cytoplasmic, light intermediate polypeptide 2
203719_at	2067	ERCC1	-0.15	0.00	excision repair cross-complementing rodent repair deficiency, complementation group 1 (includes overlapping antisense sequence)
203932_at	3109	HLA-DMB	-0.07	0.07	major histocompatibility complex, class II, DM beta /// major histocompatibility complex, class II, DM beta
204033_at	9319	TRIP13	0.36	-0.09	thyroid hormone receptor interactor 13
204066_s_at	116987	CENTG2	-0.21	-0.14	centaurin, gamma 2
204264_at	1376	CPT2	-0.04	0.03	carnitine palmitoyltransferase II
204351_at	6286	S100P	0.52	-0.14	S100 calcium binding protein P
204455_at	667	DST	0.07	0.52	dystonin
204475_at	4312	MMP1	1.32	0.42	matrix metalloproteinase 1 (interstitial collagenase)
204540_at	1917	EEF1A2	0.57	0.42	eukaryotic translation elongation factor 1 alpha 2
204589_at	9891	NUAK1	0.08	-0.05	NUAK family, SNF1-like kinase, 1
204627_s_at	3690	ITGB3	0.01	0.02	integrin, beta 3 (platelet glycoprotein IIIa, antigen CD61)
204658_at	29896	TRA2A	-0.17	-0.07	transformer-2 alpha
204916_at	10267	RAMP1	0.21	0.13	receptor (calcitonin) activity modifying protein 1
205199_at	768	CA9	0.17	-0.02	carbonic anhydrase IX
205200_at	7123	CLEC3B	-0.24	0.20	C-type lectin domain family 3, member B
205280_at	2743	GLRB	-0.04	0.27	glycine receptor, beta
205479_s_at	5328	PLAU	0.18	-0.17	plasminogen activator, urokinase
205483_s_at	9636	G1P2	0.41	-0.09	interferon, alpha-inducible protein (clone IFI-15K)
205542_at	26872	STEAP1	-0.14	0.16	six transmembrane epithelial antigen of the prostate 1
205574_x_at	649	BMP1	0.13	-0.08	bone morphogenetic protein 1
205817_at	6495	SIX1	0.25	0.09	sine oculis homeobox homolog 1 (Drosophila)
205926_at	9466	IL27RA	-0.06	0.07	interleukin 27 receptor, alpha
206022_at	4693	NDP	0.29	0.38	Norrie disease (pseudoglioma)
206100_at	1368	CPM	0.08	0.19	carboxypeptidase M
206224_at	1469	CST1	-0.04	0.34	cystatin SN
206273_at	10650	C18orf43	0.03	-0.04	chromosome 18 open reading frame 43
207069_s_at	4091	SMAD6	0.02	-0.05	SMAD, mothers against DPP homolog 6 (Drosophila)
207604_s_at	9497	SLC4A7	-0.18	0.13	solute carrier family 4, sodium bicarbonate cotransporter, member 7

207722_s_at	55643	BTBD2	-0.12	0.02	BTB (POZ) domain containing 2
207740_s_at	23636	NUP62	0.01	-0.06	nucleoporin 62kDa
207842_s_at	22794	CASC3	0.00	0.03	cancer susceptibility candidate 3
208029_s_at	55353	LAPTM4B	0.29	-0.03	lysosomal associated protein transmembrane 4 beta /// lysosomal associated protein transmembrane 4 beta
208405_s_at	8763	CD164	-0.09	-0.04	CD164 antigen, sialomucin
208424_s_at	57019	CIAPIN1	0.17	-0.04	cytokine induced apoptosis inhibitor 1
208615_s_at	8073	PTP4A2	-0.21	0.01	protein tyrosine phosphatase type IVA, member 2
208616_s_at	8073	PTP4A2	-0.05	0.06	protein tyrosine phosphatase type IVA, member 2
208636_at	87	ACTN1	0.07	-0.10	Actinin, alpha 1
208643_s_at	7520	XRCC5	-0.08	-0.03	X-ray repair complementing defective repair in Chinese hamster cells 5 (double-strand-break rejoining; Ku autoantigen, 80kDa)
208654_s_at	8763	CD164	-0.09	-0.02	CD164 antigen, sialomucin
208726_s_at	8894	EIF2S2	0.14	-0.04	eukaryotic translation initiation factor 2, subunit 2 beta, 38kDa
208767_s_at	55353	LAPTM4B	0.27	0.00	lysosomal associated protein transmembrane 4 beta
208788_at	60481	ELOVL5	-0.35	0.15	ELOVL family member 5, elongation of long chain fatty acids (FEN1/Elo2, SUR4/Elo3-like, yeast)
208836_at	483	ATP1B3	0.11	-0.02	ATPase, Na+/K+ transporting, beta 3 polypeptide
208945_s_at	8678	BECN1	-0.09	-0.02	beclin 1 (coiled-coil, myosin-like BCL2 interacting protein)
208961_s_at	1316	KLF6	0.06	-0.06	Kruppel-like factor 6
208968_s_at	57019	CIAPIN1	0.13	-0.06	cytokine induced apoptosis inhibitor 1
208998_at	7351	UCP2	-0.16	-0.01	uncoupling protein 2 (mitochondrial, proton carrier)
209189_at	2353	FOS	-0.39	-0.04	v-fos FBJ murine osteosarcoma viral oncogene homolog
209260_at	2810	SFN	0.13	-0.01	stratifin
209312_x_at	3123	HLA-DRB1	-0.29	-0.01	major histocompatibility complex, class II, DR beta 1 /// major histocompatibility complex, class II, DR beta 1
209380_s_at	10057	ABCC5	0.14	-0.02	ATP-binding cassette, sub-family C (CFTR/MRP), member 5
209427_at	6525	SMTN	0.02	-0.05	smoothelin
209619_at	972	CD74	-0.35	-0.04	CD74 antigen (invariant polypeptide of major histocompatibility complex, class II antigen-associated)
209632_at	5523	PPP2R3A	0.08	0.02	protein phosphatase 2 (formerly 2A), regulatory subunit B", alpha
209803_s_at	7262	PHLDA2	0.34	0.01	pleckstrin homology-like domain, family A, member 2
209884_s_at	9497	SLC4A7	-0.18	0.12	solute carrier family 4, sodium bicarbonate cotransporter, member 7
210095_s_at	3486	IGFBP3	0.05	-0.21	insulin-like growth factor binding protein 3
210616_s_at	22872	SEC31L1	-0.02	-0.15	SEC31-like 1 (S. cerevisiae)
211065_x_at	5211	PFKL	0.07	-0.06	phosphofructokinase, liver /// phosphofructokinase, liver
211162_x_at	6319	SCD	0.15	0.10	stearoyl-CoA desaturase (delta-9-desaturase)
211320_s_at	10076	PTPRU	0.14	-0.04	protein tyrosine phosphatase, receptor type, U
211596_s_at	26018	LRIG1	-0.53	0.02	leucine-rich repeats and immunoglobulin-like domains 1 /// leucine-rich repeats and immunoglobulin-like domains 1
211676_s_at	3459	IFNGR1	-0.01	0.00	interferon gamma receptor 1 /// interferon gamma receptor 1
211719_x_at	2335	FN1	0.04	-0.22	fibronectin 1 /// fibronectin 1

211733_x_at	6342	SCP2	-0.14	-0.03	sterol carrier protein 2 /// sterol carrier protein 2
211742_s_at	2124	EVI2B	0.00	0.13	ecotropic viral integration site 2B /// ecotropic viral integration site 2B
211880_x_at	56114	PCDHGA1	0.03	-0.02	protocadherin gamma subfamily A, 1
211937_at	1975	EIF4B	-0.19	0.00	eukaryotic translation initiation factor 4B
211943_x_at	7178	TPT1	-0.04	0.07	tumor protein, translationally-controlled 1
211963_s_at	10092	ARPC5	0.13	-0.06	actin related protein 2/3 complex, subunit 5, 16kDa
211964_at	1284	COL4A2	-0.03	-0.22	collagen, type IV, alpha 2
211974_x_at	3516	RBPSUH	0.05	-0.08	recombining binding protein suppressor of hairless (Drosophila)
211980_at	1282	COL4A1	0.01	-0.21	collagen, type IV, alpha 1
211981_at	1282	COL4A1	0.05	-0.14	collagen, type IV, alpha 1
211990_at	3113	HLA-DPA1	-0.34	-0.03	major histocompatibility complex, class II, DP alpha 1
212002_at	26099	C1orf144	-0.09	-0.07	chromosome 1 open reading frame 144
212081_x_at	7916	BAT2	-0.03	-0.09	HLA-B associated transcript 2
212143_s_at	3486	IGFBP3	0.07	-0.15	insulin-like growth factor binding protein 3
212195_at	3572	IL6ST	-0.28	0.09	Interleukin 6 signal transducer (gp130, oncostatin M receptor)
212250_at	92140	MTDH	0.13	-0.10	metadherin
212251_at	92140	MTDH	0.09	-0.13	metadherin
212265_at	9444	QKI	0.07	-0.08	quaking homolog, KH domain RNA binding (mouse)
212318_at	23534	TNPO3	0.05	-0.09	transportin 3
212619_at	23306	KIAA0286	0.13	0.04	KIAA0286 protein
212687_at	3987	LIMS1	0.04	-0.15	LIM and senescent cell antigen-like domains 1
212869_x_at	7178	TPT1	-0.03	0.03	tumor protein, translationally-controlled 1
212872_s_at	9477	TRFP	0.07	-0.02	Trf (TATA binding protein-related factor)-proximal homolog (Drosophila)
212911_at			-0.15	0.03	
213080_x_at	6125	RPL5	-0.10	-0.01	ribosomal protein L5
213151_s_at	989	SEP7	0.07	-0.06	septin 7
213628_at	23155	MCLC	-0.14	-0.06	Mid-1-related chloride channel 1
213733_at	4542	MYO1F	-0.10	-0.01	myosin IF
214150_x_at	8992	ATP6V0E	0.09	-0.02	ATPase, H+ transporting, lysosomal 9kDa, V0 subunit e
214201_x_at	7916	BAT2	0.00	-0.05	HLA-B associated transcript 2
214435_x_at	5898	RALA	0.14	-0.21	v-ral simian leukemia viral oncogene homolog A (ras related)
214848_at	7534	YWHAZ	0.10	-0.02	Tyrosine 3-monooxygenase/tryptophan 5-monooxygenase activation protein, zeta polypeptide
215235_at	6709	SPTAN1	-0.21	-0.03	Spectrin, alpha, non-erythrocytic 1 (alpha-fodrin)
215395_x_at	154754	TRY6	-0.01	-0.01	trypsinogen C
216060_s_at	23002	DAAM1	0.11	-0.09	dishevelled associated activator of morphogenesis 1
216384_x_at	440085	LOC440085	-0.03	-0.12	similar to prothymosin alpha
217729_s_at	166	AES	-0.15	0.01	amino-terminal enhancer of split
217731_s_at	9445	ITM2B	-0.11	0.00	integral membrane protein 2B
217732_s_at	9445	ITM2B	-0.14	0.01	integral membrane protein 2B
217767_at	718	C3	-0.35	-0.01	complement component 3
217838_s_at	51466	EVL	-0.41	0.12	Enah/Vasp-like
217849_s_at	9578	CDC42BPB	-0.15	-0.08	CDC42 binding protein kinase beta (DMPK-like)
217998_at	22822	PHLDA1	0.06	-0.02	pleckstrin homology-like domain, family A, member 1
218036_x_at	51068	NMD3	0.16	-0.05	NMD3 homolog (S. cerevisiae)

218168_s_at	56997	CABC1	-0.01	0.06	chaperone, ABC1 activity of bc1 complex like (S. pombe)
218173_s_at	54904	WHSC1L1	0.12	-0.01	Wolf-Hirschhorn syndrome candidate 1-like 1
218322_s_at	51703	ACSL5	-0.13	0.07	acyl-CoA synthetase long-chain family member 5
218589_at	10161	P2RY5	-0.17	-0.01	purinergic receptor P2Y, G-protein coupled, 5
218650_at	54487	DGCR8	-0.08	-0.02	DiGeorge syndrome critical region gene 8
218693_at	23555	TSPAN15	-0.08	0.10	tetraspanin 15
218723_s_at	28984	RGC32	-0.19	-0.06	response gene to complement 32
218755_at	10112	KIF20A	0.37	-0.12	kinesin family member 20A
218758_s_at	8568	D21S2056E	0.03	-0.06	DNA segment on chromosome 21 (unique) 2056 expressed sequence
218795_at	51205	ACP6	-0.16	0.02	acid phosphatase 6, lysophosphatidic
218901_at	57088	PLSCR4	-0.22	-0.02	phospholipid scramblase 4
218915_at	4771	NF2	-0.11	-0.04	neurofibromin 2 (bilateral acoustic neuroma)
219427_at	79633	FAT4	-0.09	-0.01	FAT tumor suppressor homolog 4 (Drosophila)
220753_s_at	51084	CRYL1	-0.20	0.00	crystallin, lambda 1
221123_x_at	55893	ZNF395	-0.28	0.07	zinc finger protein 395
221272_s_at	81563	C1orf21	-0.15	0.09	chromosome 1 open reading frame 21 /// chromosome 1 open reading frame 21
221485_at	9334	B4GALT5	0.13	-0.10	UDP-Gal:betaGlcNAc beta 1,4-galactosyltransferase, polypeptide 5
221741_s_at	54915	YTHDF1	0.09	-0.06	YTH domain family, member 1
221771_s_at	54737	HSMPP8	-0.16	0.06	M-phase phosphoprotein, mpp8
221841_s_at	9314	KLF4	-0.16	0.13	Kruppel-like factor 4 (gut)
222062_at	9466	IL27RA	-0.08	0.13	interleukin 27 receptor, alpha
222327_x_at	283491	OR7E156P	0.02	-0.02	olfactory receptor, family 7, subfamily E, member 156 pseudogene
32029_at	5170	PDPK1	0.00	-0.01	3-phosphoinositide dependent protein kinase-1
33323_r_at	2810	SFN	0.09	-0.15	stratifin
40850_at	23770	FKBP8	-0.08	0.02	FK506 binding protein 8, 38kDa
46665_at	54910	SEMA4C	-0.02	-0.09	sema domain, immunoglobulin domain (Ig), transmembrane domain (TM) and short cytoplasmic domain, (semaphorin) 4C

List of the microarray probes selected in the Fra1 classifier. The values of the poor and good prognostic centroids are also displayed.

Supplementary Table 2: Primers used for RT-PCR experiments

Gene	Forward primer sequence (5'-3')	Reverse primer sequence (5'-3')
Rat Fra-1	GCAGACACAGACAGTCCAG	CCATCCACTGCAATTCCTG
Rat HPRT1	CTGGTGAAAAGGACCTCTCG	TGAAGTGCTCATTATAGTCAAGGGCA
Human ADORA1	CCGGGTCAAGATCCCTCT	AGTCCCACCACGAAGGAGA
Human ADORA2A	GGAGGGCTGTCAGGTGAA	GTTCTGGCAGCAGCATCAT-
Human ADORA2B	TCTGTGTCCCGCTCAGGT	GATGCCAAAGGCAAGGAC
Human ADORA3	TCTCCTTGGCTCTCATTTCAG	GTAGTGGGCATTGTAGTTGCAG
Human beta-Actin	CCAACCGCGAGAAGATGA	CCAGAGGCGTACAGGGATAG

Sequences of the primer sets used for RT-PCR experiments

Supplementary Table 3: Primers used for ChIP experiments

Primer set	Forward primer sequence (5'-3')	Reverse primer sequence (5'-3')
Negative Control 1	GGTCTGCCTTCTACTTTCCAA	TGGTATTTAAAAATCCTAACGGTTG
Negative Control 2	ACATACTCTTTGTACTCAGAATTTCCA	TAATGACAGAATAAGGATTGGAACC
Site 1	ATTTGTGACAGGCCTCATCC	CAAACAATTCCAGAGCGAGAG
Site 2	CTGCAGAACTGTGAGCCAAA	TCACCATTTCCCCTTTTCAG
Site 3	AGCCTGCTTCAGGTTTACCA	AATGCAGGAAATGCTGGAAC
Site 4	CTGGAGCCACAATCAGTGAG	CTCTTGAACCTGTCCCGTGT
Site 5	AACGAAGTTTGTGGTTTCAGA	TGCCAGTGTATGTGTGTGTGA

Sequences of the primer sets used for ChIP experiments

Supplementary references

1. Loi S*, et al.* (2007) Definition of clinically distinct molecular subtypes in estrogen receptor-positive breast carcinomas through genomic grade. *J Clin Oncol* 25(10):1239-1246.
2. Miller LD*, et al.* (2005) An expression signature for p53 status in human breast cancer predicts mutation status, transcriptional effects, and patient survival. *Proc Natl Acad Sci USA* 102:13550-13555.
3. Pawitan Y*, et al.* (2005) Gene expression profiling spares early breast cancer patients from adjuvant therapy: derived and validated in two population-based cohorts. *Breast Cancer Res* 7(6):R953 - R964.
4. Desmedt C*, et al.* (2007) Strong Time Dependence of the 76-Gene Prognostic Signature for Node-Negative Breast Cancer Patients in the TRANSBIG Multicenter Independent Validation Series. *Clin Cancer Res* 13(11):3207-3214.
5. Minn AJ*, et al.* (2005) Genes that mediate breast cancer metastasis to lung. *Nature* 436(7050):518-524.
6. Chin K*, et al.* (2006) Genomic and transcriptional aberrations linked to breast cancer pathophysiologies. *Cancer Cell* 10(6):529-541.
7. Legutko A*, et al.* (2011) Sirtuin 1 promotes Th2 responses and airway allergy by repressing peroxisome proliferator-activated receptor-γ activity in dendritic cells. *J Immunol* 187(9):4517-4529.
8. Smit MA, Geiger TR, Song JY, Gitelman I, & Peeper DS (2009) A Twist-Snail axis critical for TrkB-induced epithelial-mesenchymal transition-like transformation, anoikis resistance, and metastasis. *Mol Cell Biol* 29(13):3722-3737.

9. Schmidt D*, et al.* (2009) ChIP-seq: using high-throughput sequencing to discover protein-DNA interactions. *Methods* 48(3):240-248.

10. Brummelkamp TR, Bernards R, & Agami R (2002) Stable suppression of tumorigenicity by virus-mediated RNA interference. *Cancer Cell* 2(3):243-247.

11. Ivanova N*, et al.* (2006) Dissecting self-renewal in stem cells with RNA interference. *Nature* 442(7102):533-538.

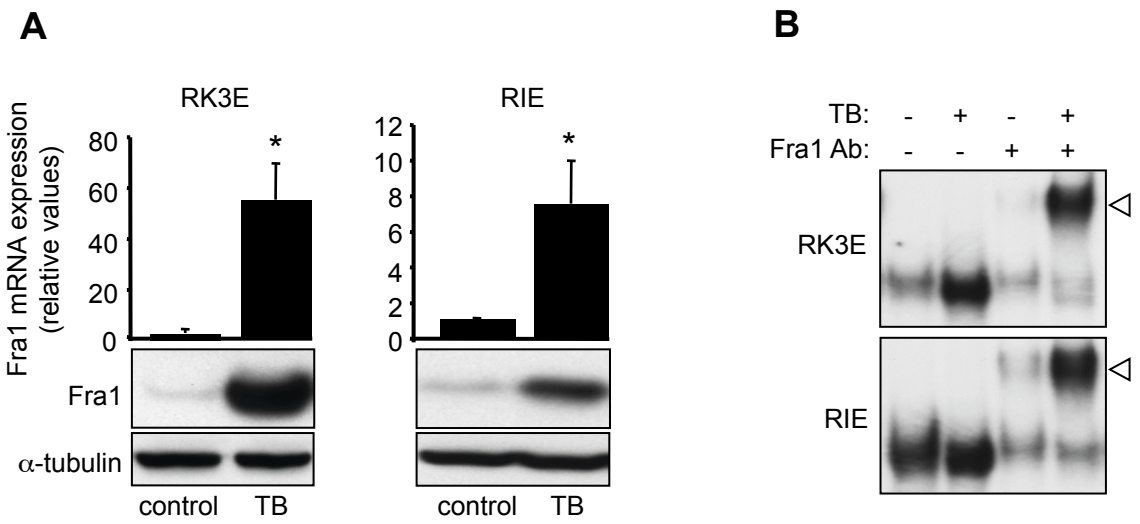
A
RK3E
RIE
Fra1 mRNA expression
(relative values)
80
60
40
20
0
12
10
8
6
4
2
0
*
*
Fra1
α-tubulin
control
TB
control
TB
B
TB: - + - +
Fra1 Ab: - - + +
RK3E
RIE

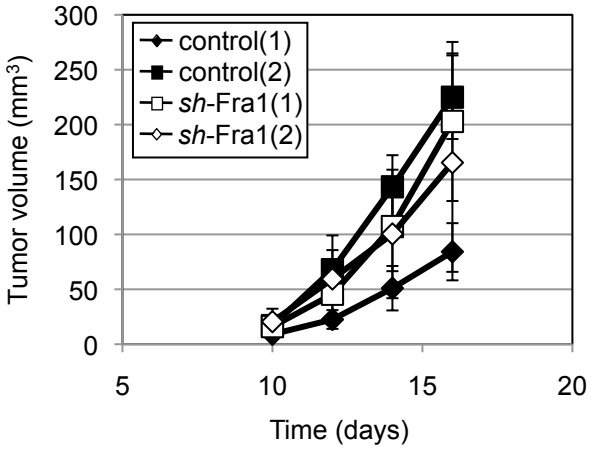
300
250
200
150
100
50
0
Tumor volume (mm3)
control(1)
control(2)
sh-Fra1(1)
sh-Fra1(2)
5
10
15
20
Time (days)

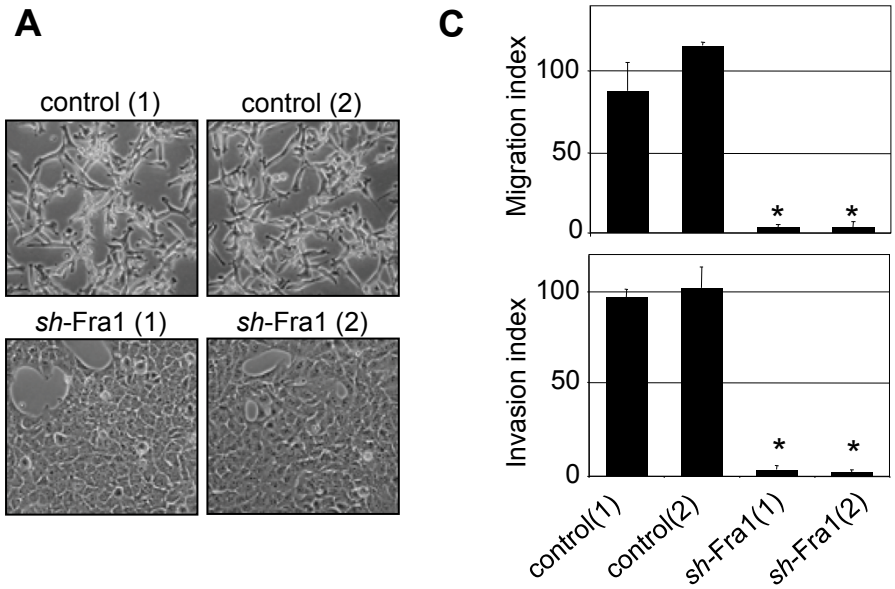
A
control (1)
control (2)
sh-Fra1 (1)
sh-Fra1 (2)
C
Migration index
100
50
0
*
*
Invasion index
100
50
0
*
*
control(1)
control(2)
sh-Fra1(1)
sh-Fra1(2)

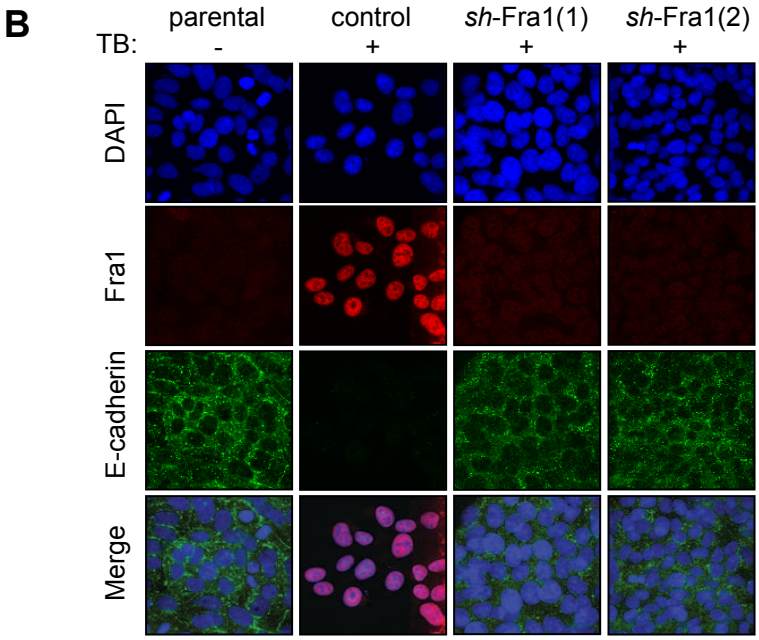
B
TB:
parental
-
control
+
sh-Fra1(1)
+
sh-Fra1(2)
+
DAPI
Fra1
E-cadherin
Merge

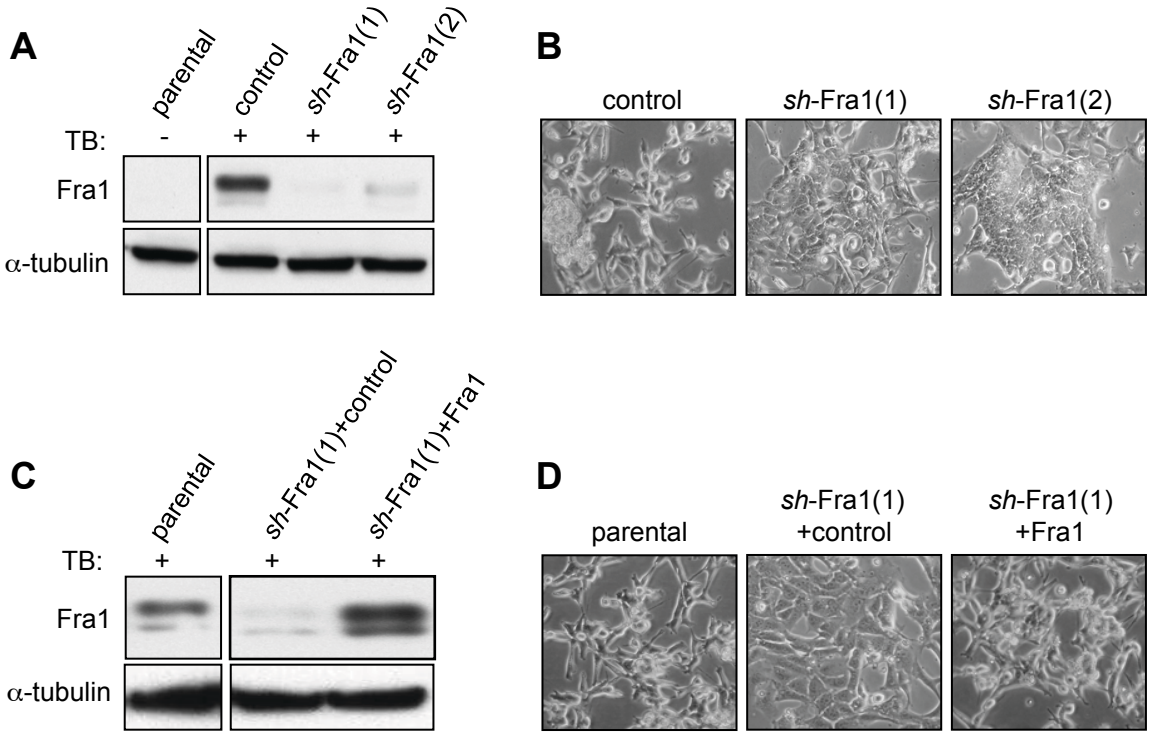
A
parental
control
sh-Fra1(1)
sh-Fra1(2)
TB:
-
+
+
+
Fra1
α-tubulin
B
control
sh-Fra1(1)
sh-Fra1(2)
C
parental
sh-Fra1(1)+control
sh-Fra1(1)+Fra1
TB:
+
+
+
Fra1
α-tubulin
D
parental
sh-Fra1(1)
+control
sh-Fra1(1)
+Fra1

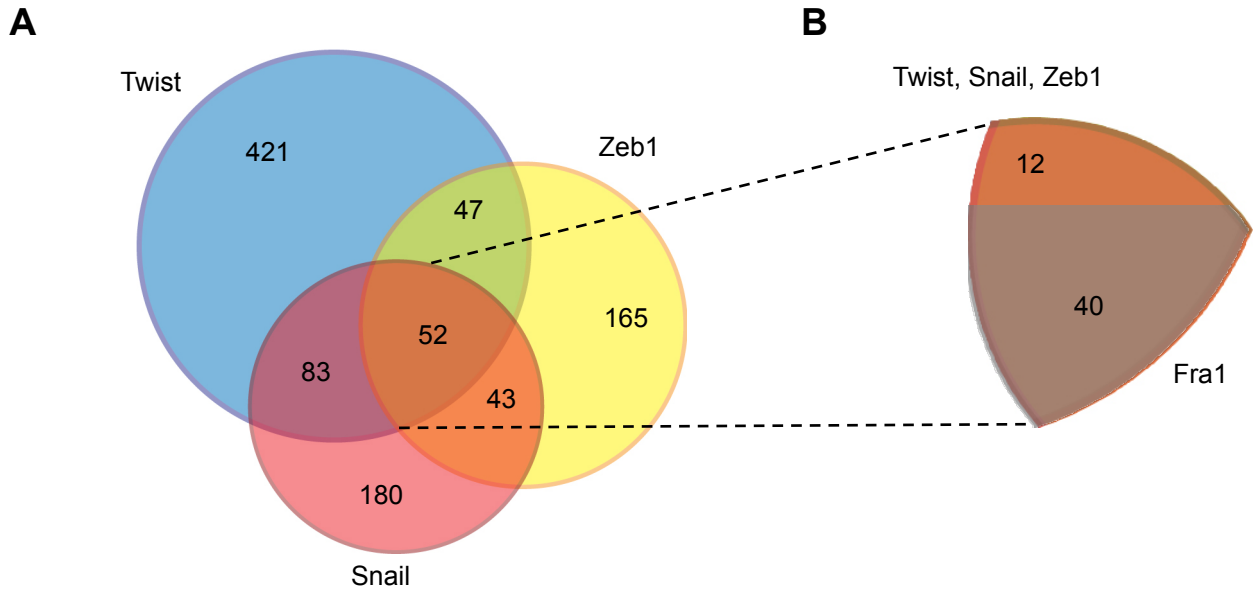
A
Twist
421
Zeb1
47
165
52
83
43
180
Snail
B
Twist, Snail, Zeb1
12
40
Fra1

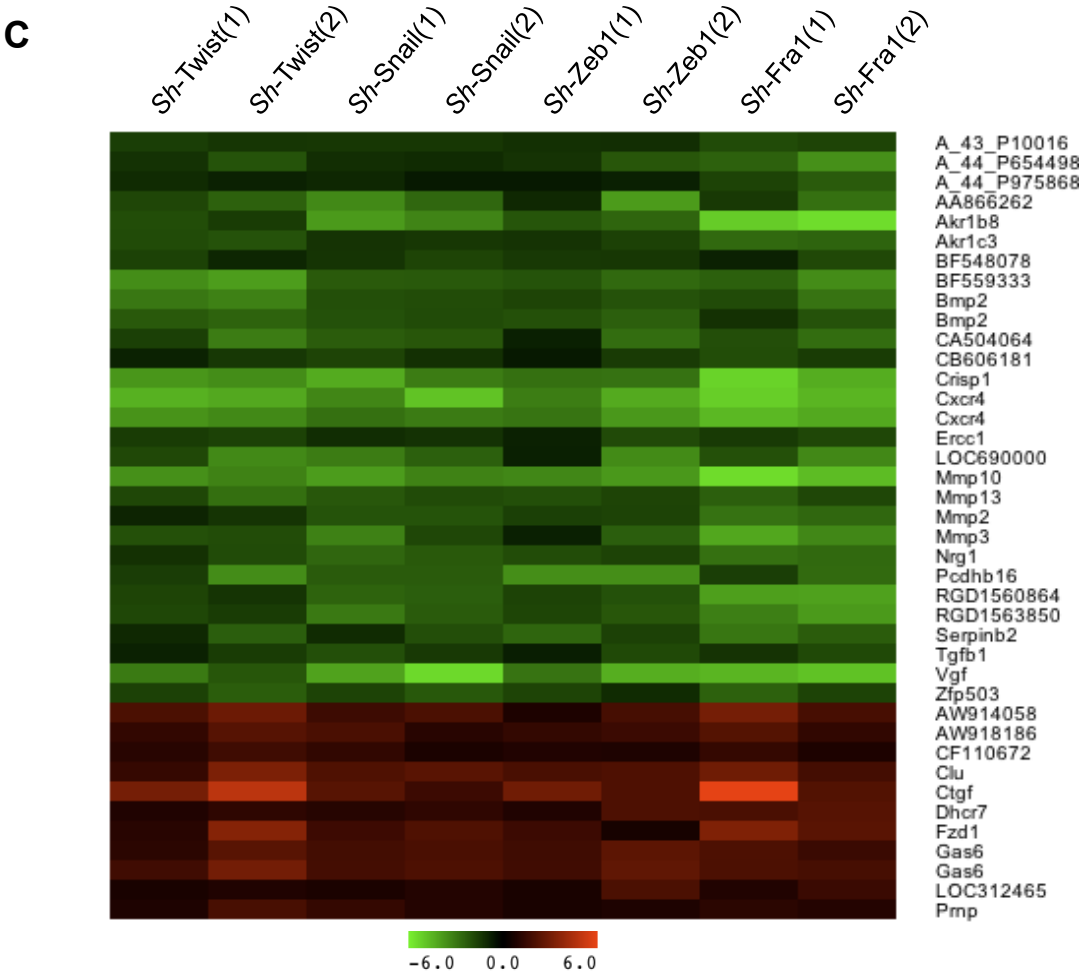
C
Sh-Twist(1)
Sh-Twist(2)
Sh-Snail(1)
Sh-Snail(2)
Sh-Zeb1(1)
Sh-Zeb1(2)
Sh-Fra1(1)
Sh-Fra1(2)
A_43_P10016
A_44_P654498
A_44_P975868
AA866262
Akr1b8
Akr1c3
BF548078
BF559333
Bmp2
Bmp2
CA504064
CB606181
Crisp1
Cxcr4
Cxcr4
Ercc1
LOC690000
Mmp10
Mmp13
Mmp2
Mmp3
Nrg1
Pcdhb16
RGD1560864
RGD1563850
Serpinb2
Tgfb1
Vgf
Zfp503
AW914058
AW918186
CF110672
Clu
Ctgf
Dhcr7
Fzd1
Gas6
Gas6
LOC312465
Pmp
-6.0
0.0
6.0

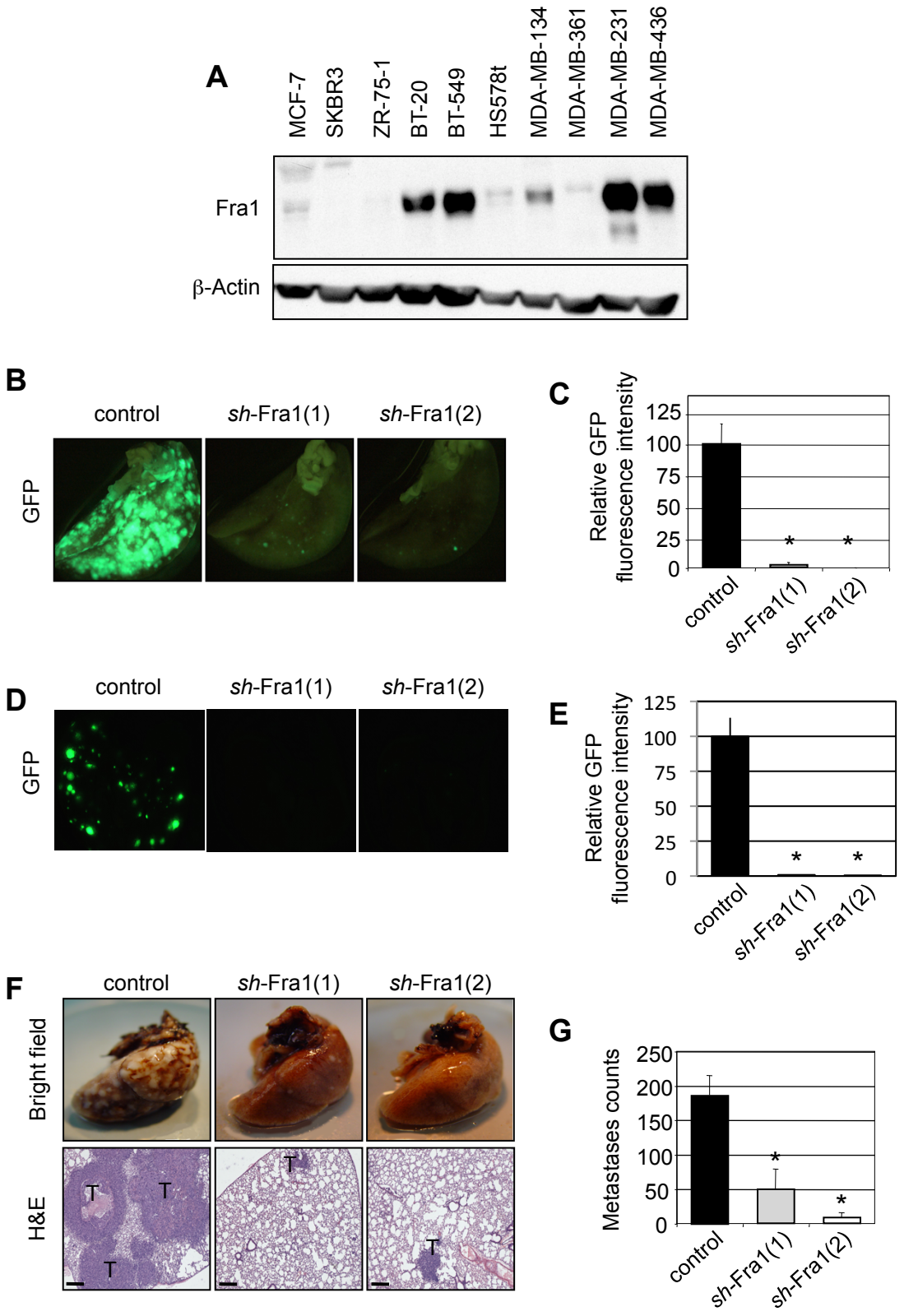
A
MCF-7
SKBR3
ZR-75-1
BT-20
BT-549
HS578t
MDA-MB-134
MDA-MB-361
MDA-MB-231
MDA-MB-436
Fra1
β-Actin
B
control
sh-Fra1(1)
sh-Fra1(2)
GFP
C
Relative GFP fluorescence intensity
125
100
75
50
25
0
control
sh-Fra1(1)
sh-Fra1(2)
D
control
sh-Fra1(1)
sh-Fra1(2)
GFP
E
Relative GFP fluorescence intensity
125
100
75
50
25
0
control
sh-Fra1(1)
sh-Fra1(2)
F
control
sh-Fra1(1)
sh-Fra1(2)
Bright field
H&E
T
G
Metastases counts
250
200
150
100
50
0
control
sh-Fra1(1)
sh-Fra1(2)

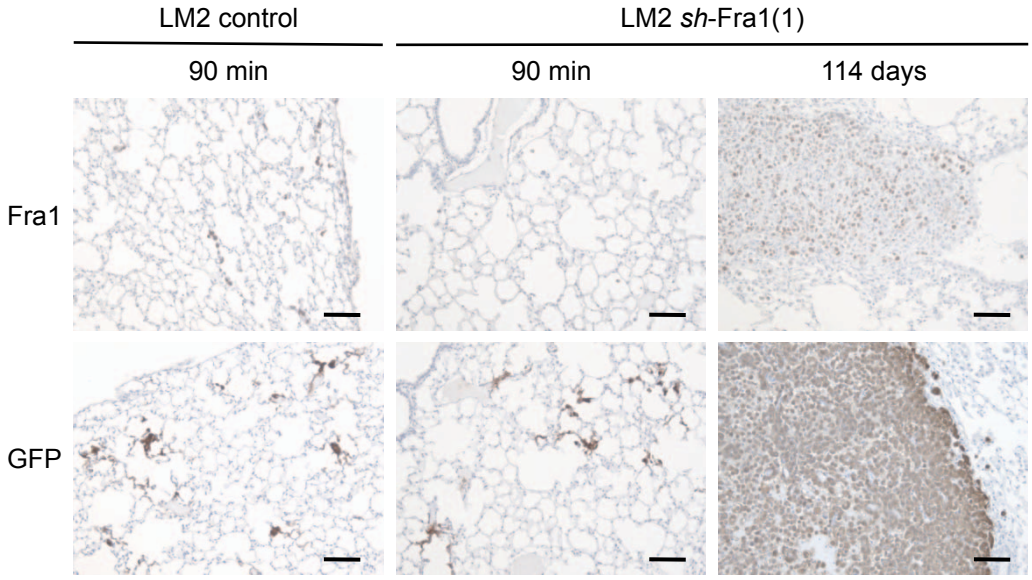
LM2 control
LM2 sh-Fra1(1)
90 min
90 min
114 days
Fra1
GFP

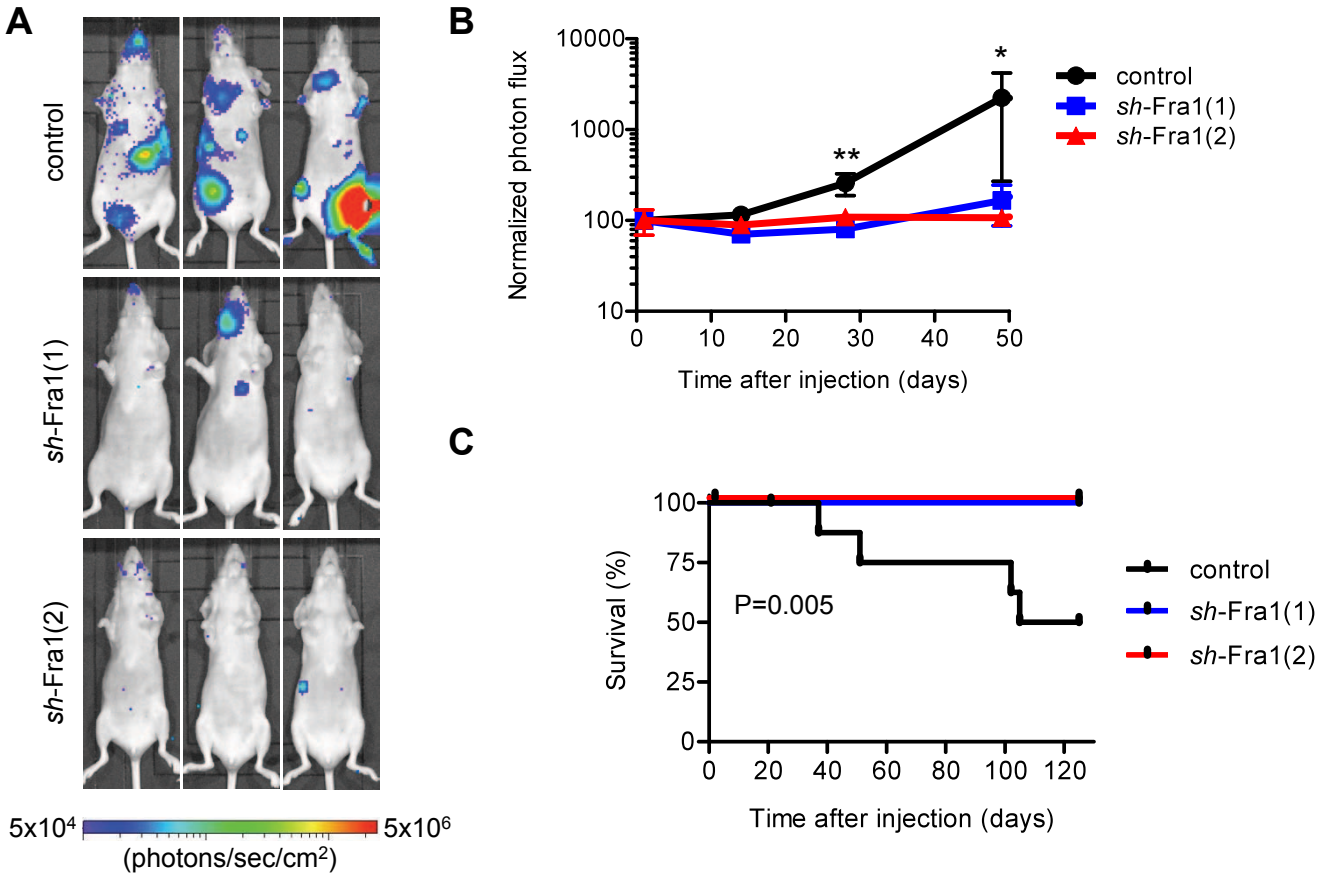

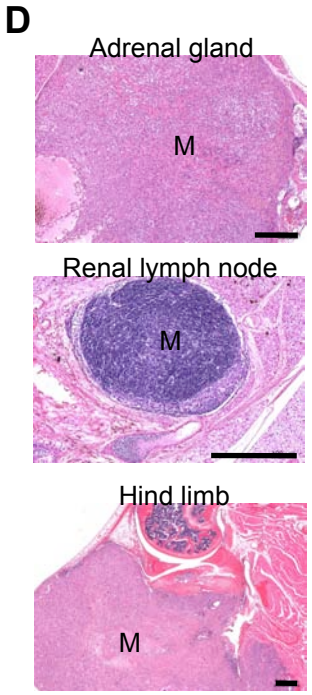

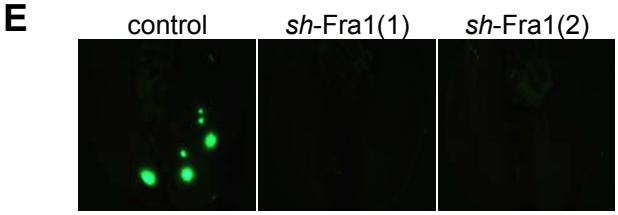

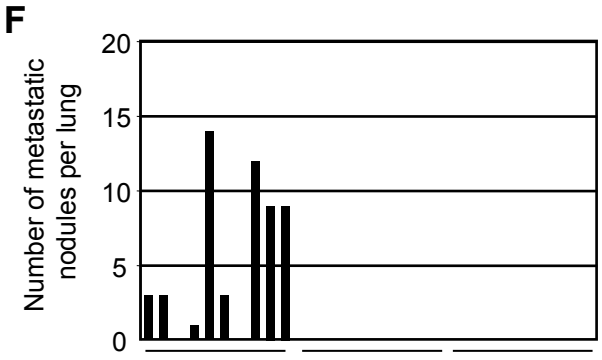

	control	*sh*-Fra1(1)	*sh*-Fra1(2)
Prevalence of lung metastasis	8/10	0/10	0/10
Average lung nodules (+/- S.D.)	5.4 (± 5.1)	0	0

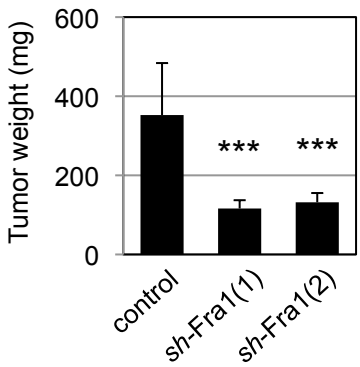

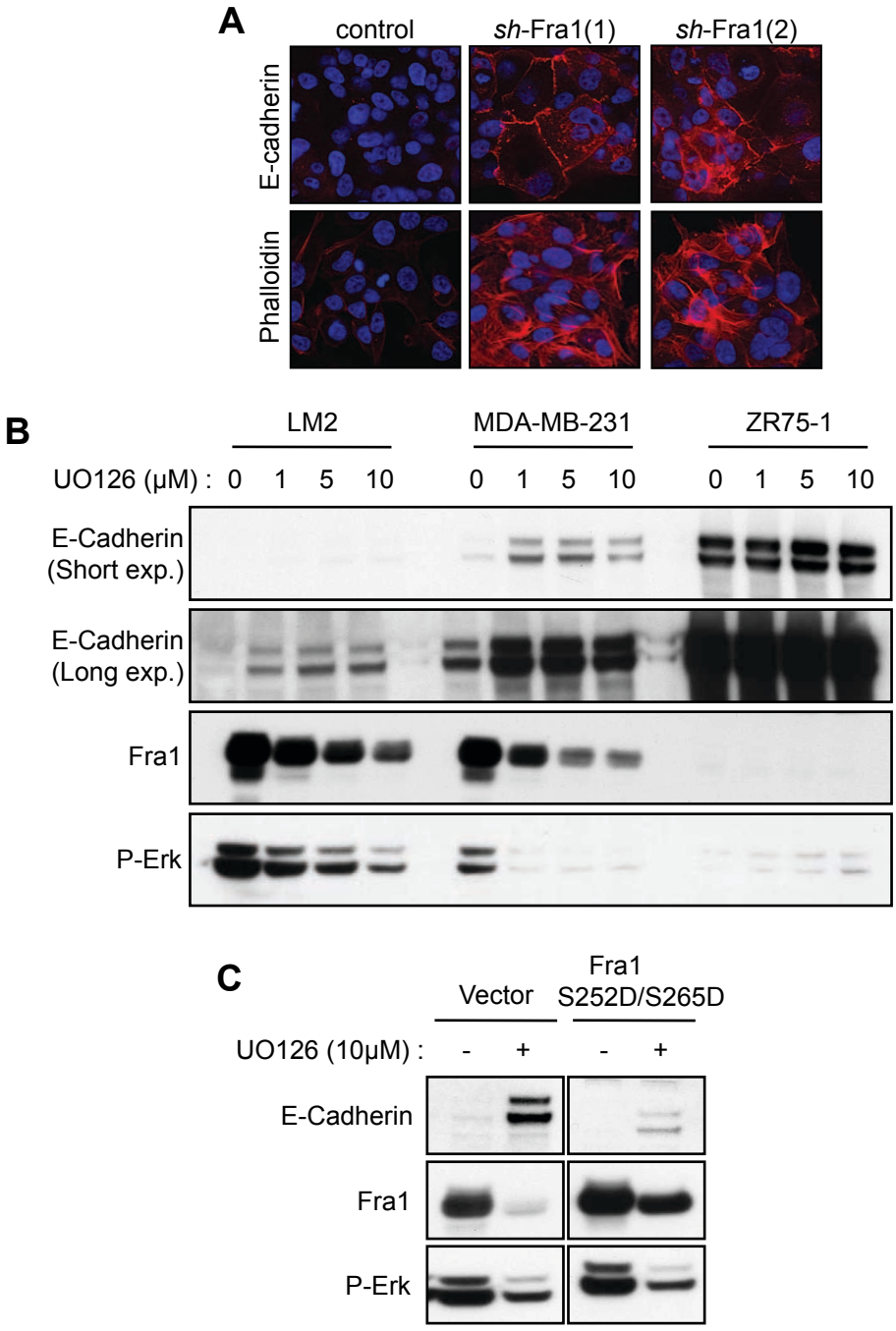
A
control
sh-Fra1(1)
sh-Fra1(2)
E-cadherin
Phalloidin
B
LM2
MDA-MB-231
ZR75-1
UO126 (μM) : 0 1 5 10 0 1 5 10 0 1 5 10
E-Cadherin (Short exp.)
E-Cadherin (Long exp.)
Fra1
P-Erk
C
Vector
Fra1 S252D/S265D
UO126 (10μM) : - + - +
E-Cadherin
Fra1
P-Erk

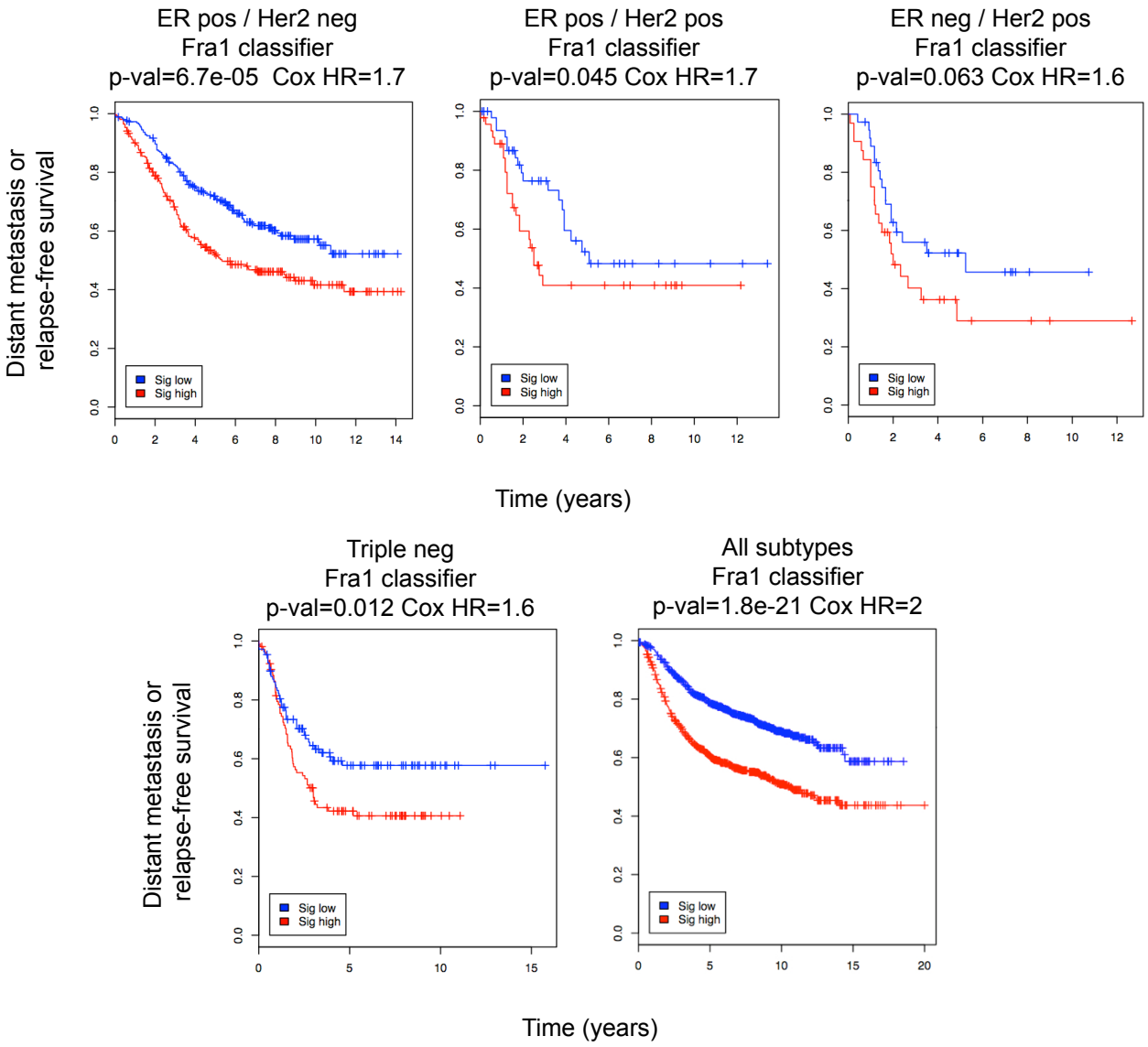
ER pos / Her2 neg
Fra1 classifier
p-val=6.7e-05 Cox HR=1.7
ER pos / Her2 pos
Fra1 classifier
p-val=0.045 Cox HR=1.7
ER neg / Her2 pos
Fra1 classifier
p-val=0.063 Cox HR=1.6
Distant metastasis or relapse-free survival
Sig low
Sig high
Time (years)
Triple neg
Fra1 classifier
p-val=0.012 Cox HR=1.6
All subtypes
Fra1 classifier
p-val=1.8e-21 Cox HR=2
Distant metastasis or relapse-free survival
Sig low
Sig high
Time (years)

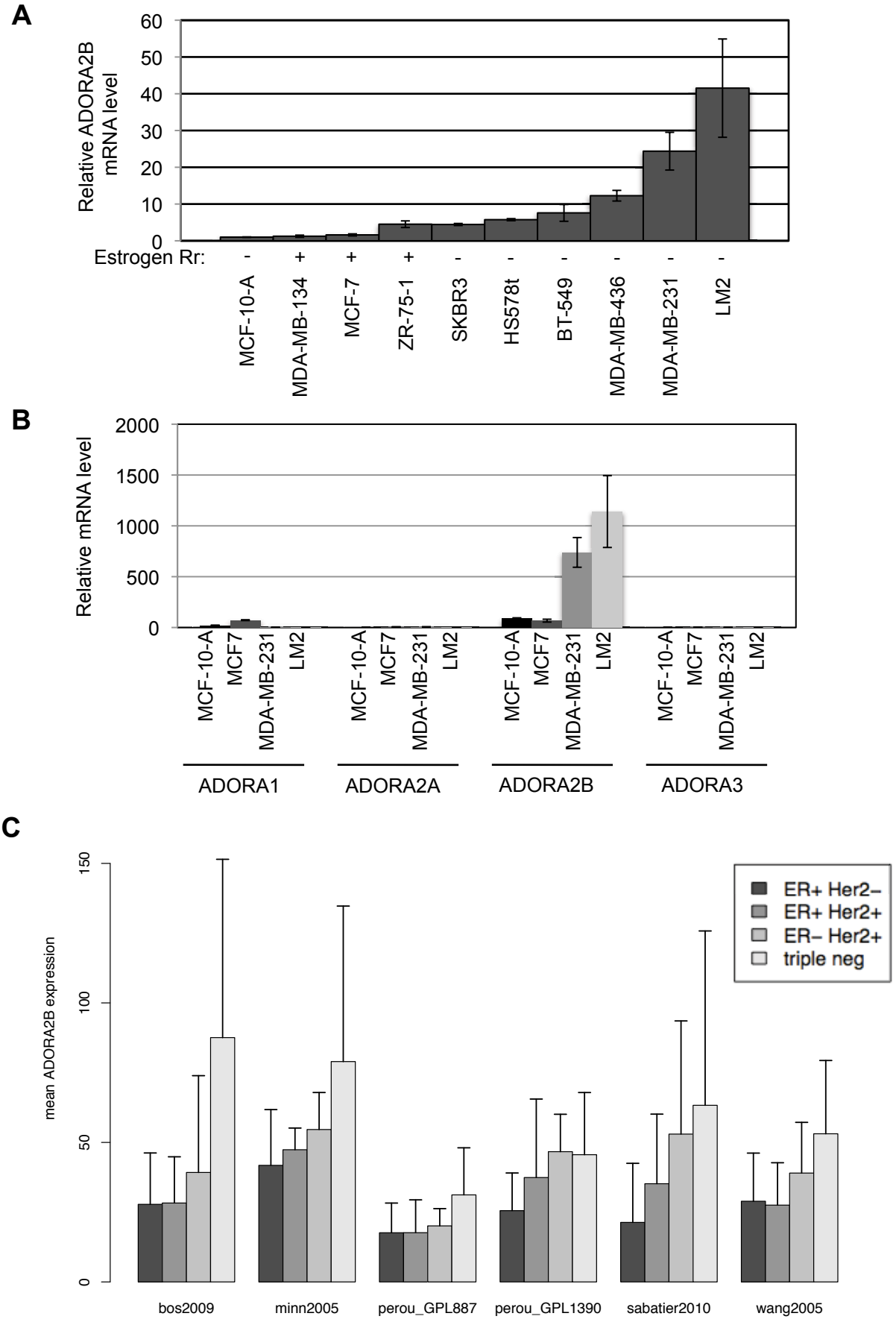
A
Relative ADORA2B mRNA level
60
50
40
30
20
10
0
Estrogen Rr: - + + + - - - - - -
MCF-10-A
MDA-MB-134
MCF-7
ZR-75-1
SKBR3
HS578t
BT-549
MDA-MB-436
MDA-MB-231
LM2
B
Relative mRNA level
2000
1500
1000
500
0
MCF-10-A
MCF7
MDA-MB-231
LM2
ADORA1
ADORA2A
ADORA2B
ADORA3
C
mean ADORA2B expression
150
100
50
0
ER+ Her2–
ER+ Her2+
ER– Her2+
triple neg
bos2009
minn2005
perou_GPL887
perou_GPL1390
sabatier2010
wang2005

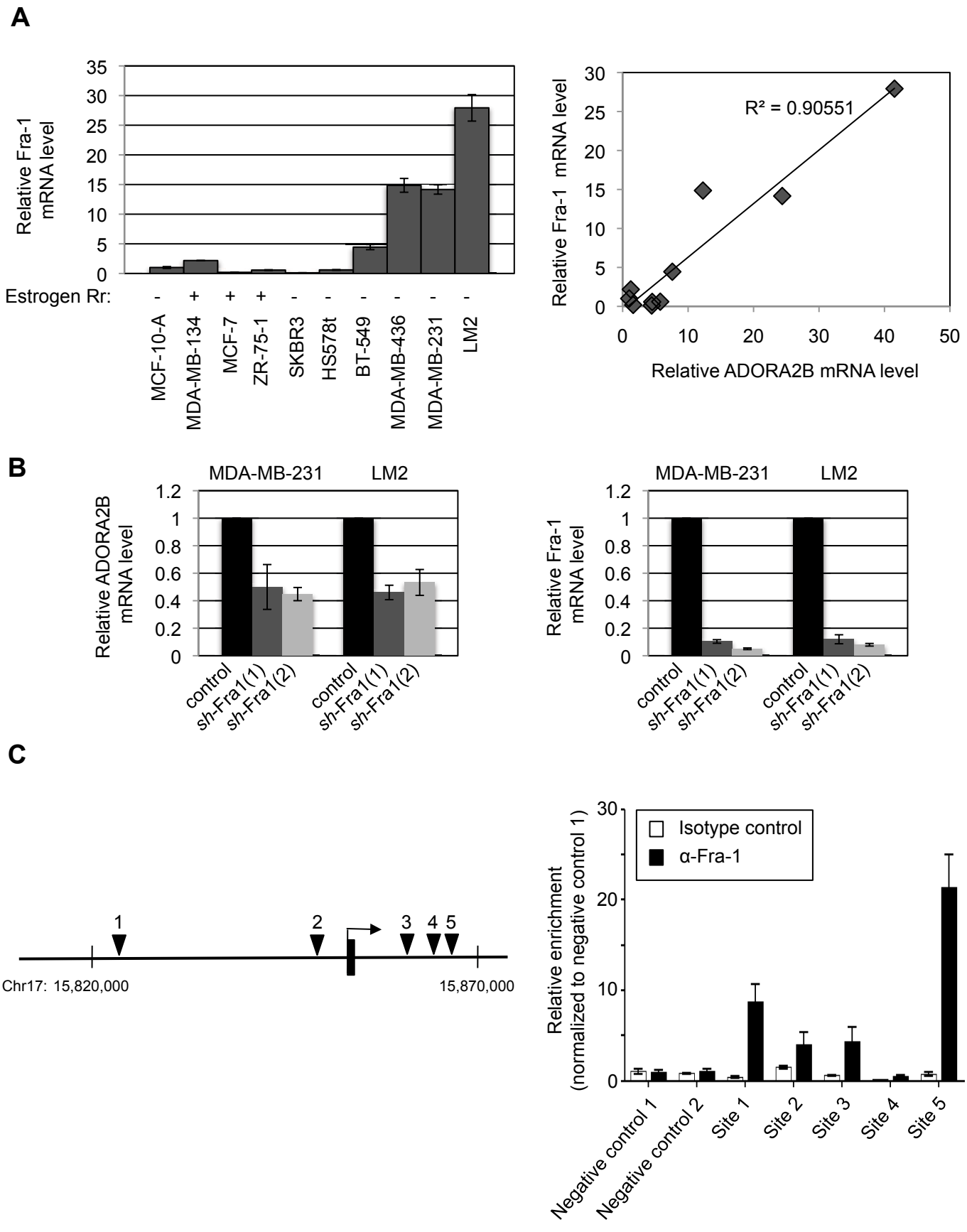
A
Relative Fra-1 mRNA level
35
30
25
20
15
10
5
0
Estrogen Rr: - + + + - - - - - -
MCF-10-A
MDA-MB-134
MCF-7
ZR-75-1
SKBR3
HS578t
BT-549
MDA-MB-436
MDA-MB-231
LM2
Relative Fra-1 mRNA level
R² = 0.90551
Relative ADORA2B mRNA level
B
MDA-MB-231
LM2
Relative ADORA2B mRNA level
control
sh-Fra1(1)
sh-Fra1(2)
Relative Fra-1 mRNA level
C
1
2
3
4
5
Chr17: 15,820,000
15,870,000
Relative enrichment (normalized to negative control 1)
Isotype control
α-Fra-1
Negative control 1
Negative control 2
Site 1
Site 2
Site 3
Site 4
Site 5

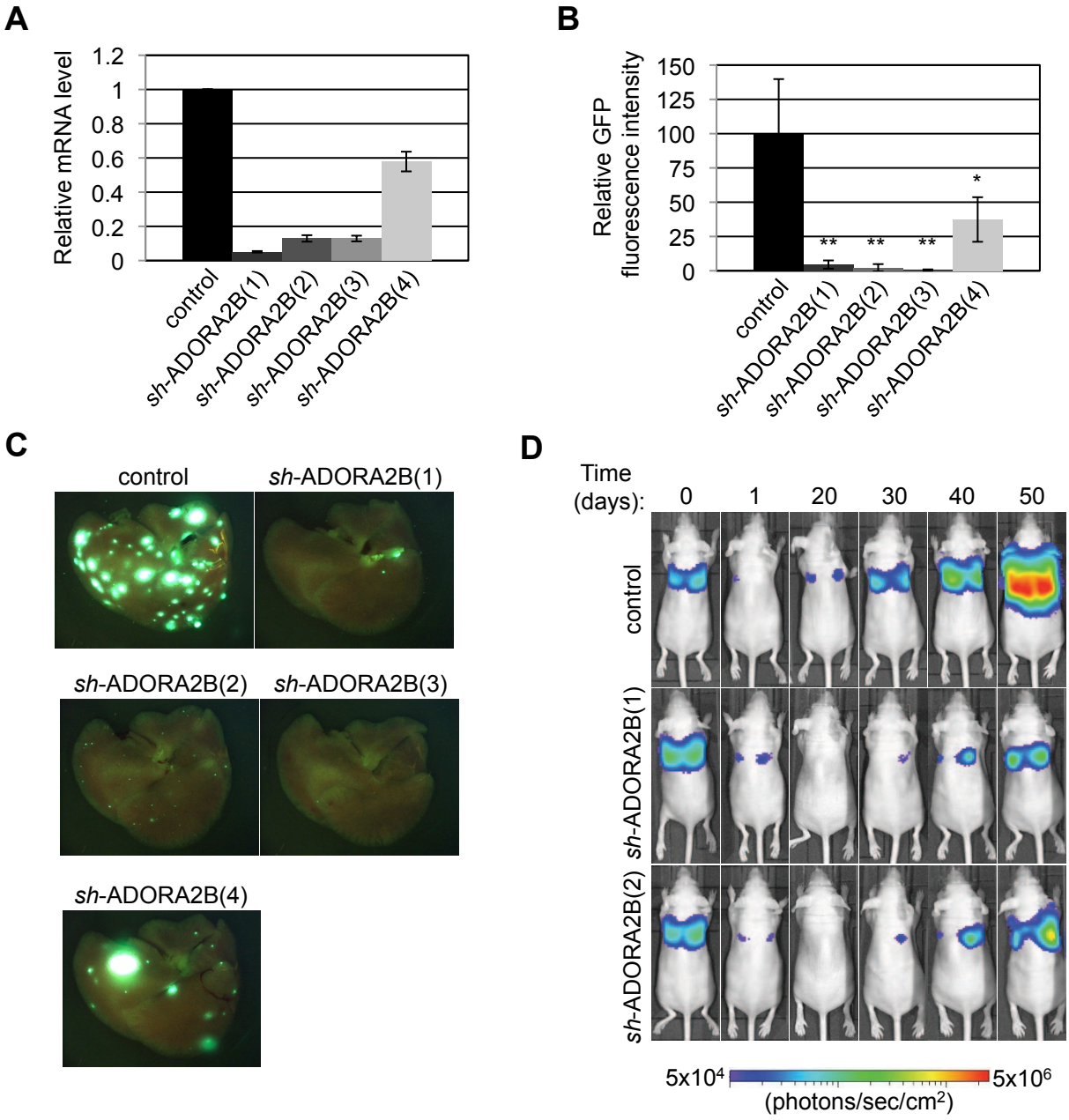
A
Relative mRNA level
1.2
1
0.8
0.6
0.4
0.2
0
control
sh-ADORA2B(1)
sh-ADORA2B(2)
sh-ADORA2B(3)
sh-ADORA2B(4)
B
Relative GFP fluorescence intensity
150
125
100
75
50
25
0
**
**
**
*
control
sh-ADORA2B(1)
sh-ADORA2B(2)
sh-ADORA2B(3)
sh-ADORA2B(4)
C
control
sh-ADORA2B(1)
sh-ADORA2B(2)
sh-ADORA2B(3)
sh-ADORA2B(4)
D
Time (days):
0
1
20
30
40
50
control
sh-ADORA2B(1)
sh-ADORA2B(2)
5x10^4
5x10^6
(photons/sec/cm^2)
E
Population doublings
50
40
30
20
10
0
control
sh-ADORA2B(1)
sh-ADORA2B(2)
0
2
4
6
8
10
Time (days)
F
Tumor volume (mm^3)
200
175
150
125
100
75
50
25
0
control
sh-ADORA2B(1)
sh-ADORA2B(2)
0
5
10
15
20
25
30
Time (days)

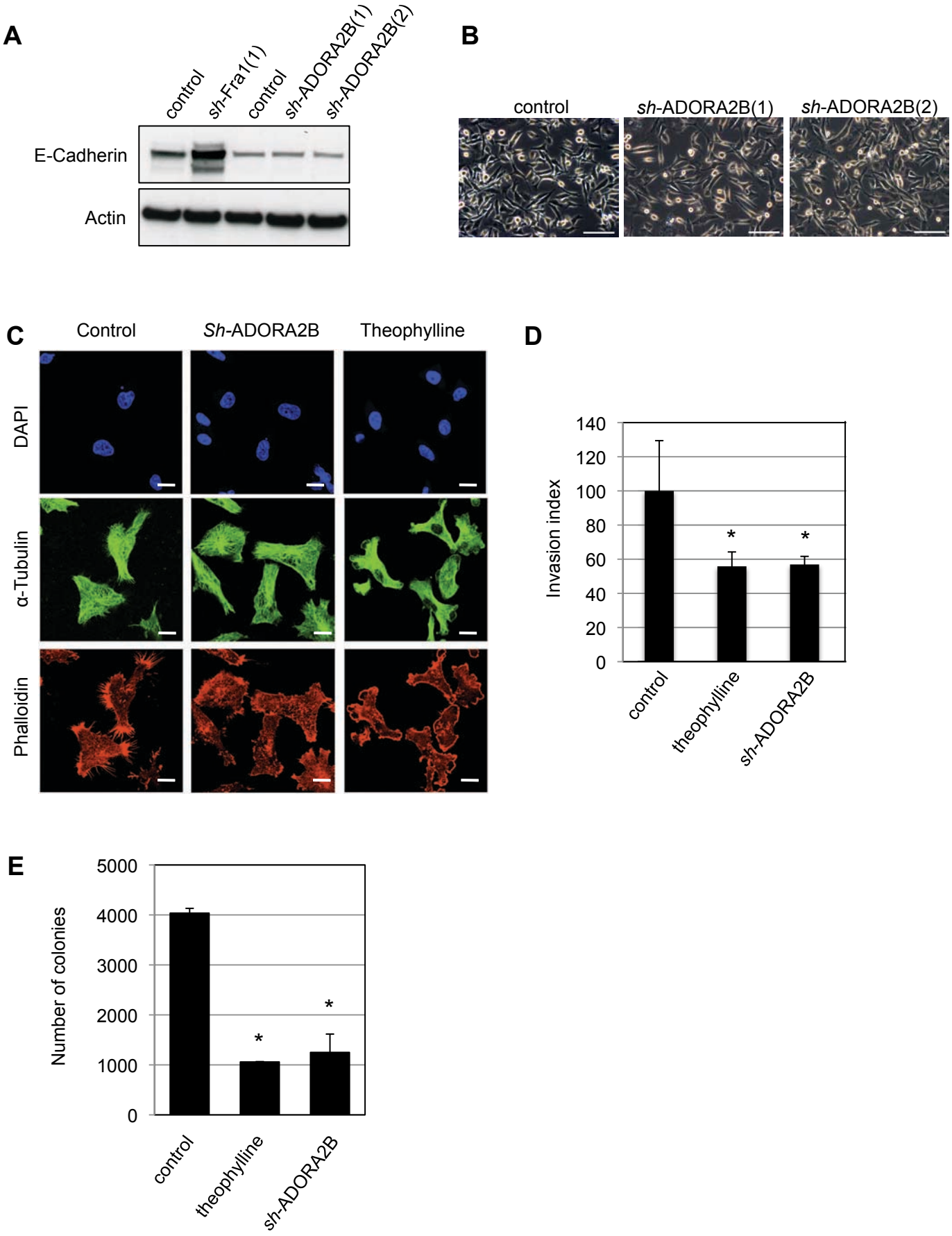
A
control
sh-Fra1(1)
control
sh-ADORA2B(1)
sh-ADORA2B(2)
E-Cadherin
Actin
B
control
sh-ADORA2B(1)
sh-ADORA2B(2)
C
Control
Sh-ADORA2B
Theophylline
DAPI
α-Tubulin
Phalloidin
D
Invasion index
140
120
100
80
60
40
20
0
*
*
control
theophylline
sh-ADORA2B
E
Number of colonies
5000
4000
3000
2000
1000
0
*
*
control
theophylline
sh-ADORA2B

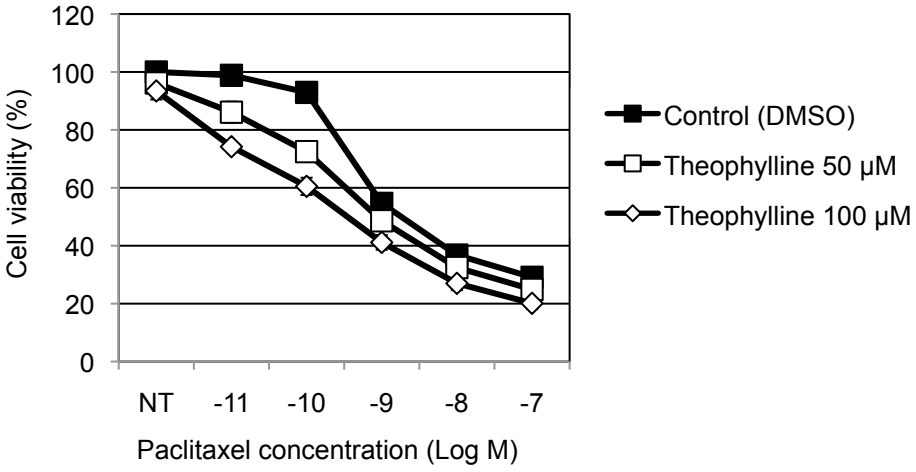
120
100
80
60
40
20
0
Cell viability (%)
NT
-11
-10
-9
-8
-7
Paclitaxel concentration (Log M)
Control (DMSO)
Theophylline 50 µM
Theophylline 100 µM

A

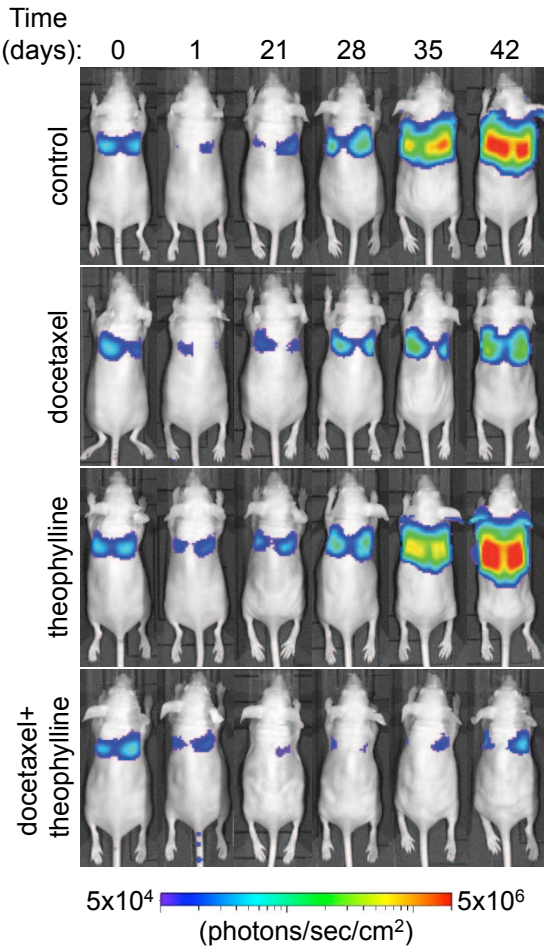
Time
(days): 0 1 21 28 35 42
control
docetaxel
theophylline
docetaxel+
theophylline
5x10⁴
5x10⁶
(photons/sec/cm²)

B

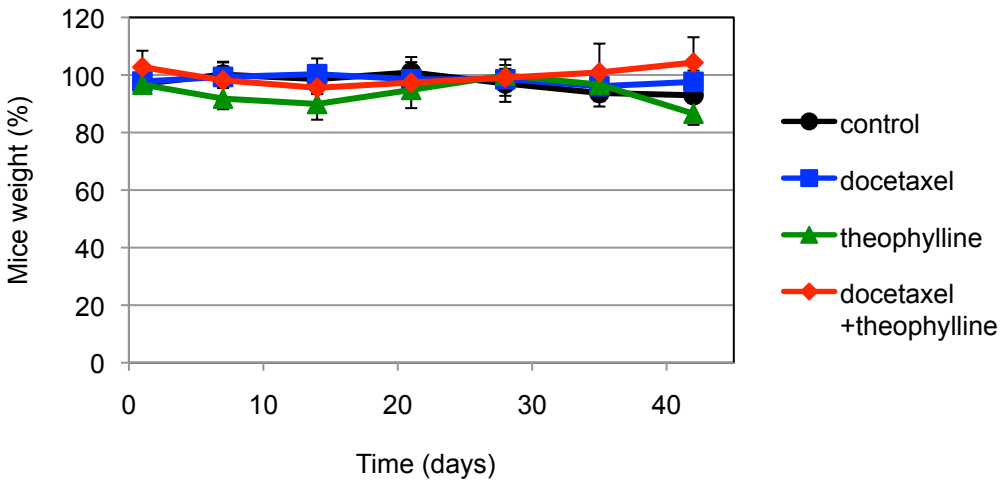
120
100
80
60
40
20
0
Mice weight (%)
0
10
20
30
40
Time (days)
control
docetaxel
theophylline
docetaxel
+theophylline

Supplementary figures legends

Supplementary Figure 1. Fra-1 is upregulated and is a major component of AP-1 DNA-binding complexes in active TrkB expressing cells. A. Fra-1 expression levels measured by quantitative RT-PCR (upper panel) and western blotting (lower panel; n for PCR = 3, error bars: S.D. Asterisk, different from control with $P < 0.01$ based on a one-sided Student's t test). **B.** Gel shift analysis measuring AP-1 DNA-binding activity. Supershift with Fra-1 antibody was performed to determine the relative contribution of Fra-1 to the total DNA-binding activity (empty arrows indicate supershifted AP-1 complex). Data are representative of three independent experiments.

Supplementary Figure 2. Fra-1 depletion does not affect the growth of primary TrkB-driven tumor xenografts. *In vivo* growth curve of tumors formed by $RK3E^{TB}$ tumor cells injected subcutaneously into nude mice, as a function of Fra-1 depletion (n=6, error bars: S.E.). Data are representative of three independent experiments.

Supplementary Figure 3. Fra-1 is required for the downregulation of epithelial characteristics, and for migration and invasion of TrkB-expressing tumor cells. A. Phase contrast micrographs showing the effects of Fra-1 depletion on the morphology of RK3ETB cells. Images were taken at 40x magnification. **B.** Detection by immunofluorescence of Fra-1 and E-cadherin in cells as indicated. Parental RK3E cells are included as reference. **C.** Migration (upper panel) and invasion (lower panel) capacities as a function of Fra-1 depletion (n=3, error bars: S.D. Asterisk, different from control clones with $P < 0.001$ based on a one-

way ANOVA followed by PLSD test). Data are representative of three independent experiments.

Supplementary Figure 4. Fra-1 depletion in RK3E^{TB} cells reverts morphological transformation. A. Fra-1 expression levels in polyclonal pools of RK3E^{TB} cells containing empty vector or independent shRNAs targeting Fra-1, as indicated. **B.** Phase contrast micrographs of the cells described in A. **C.** Restoration of an RNAi-resistant rat Fra-1 cDNA in sh-Fra1(1) expressing RK3E^{TB} cells, resulting in morphological transformation. **D.** Phase contrast micrographs of the cells described in C**.** In both A. and C., the panels were taken from a single blot and α-tubulin serves as loading control. Cells were photographed at 40x magnification. Data are representative of three independent experiments.

Supplementary Figure 5. Fra-1 and the EMT regulators Twist, Snail and Zeb1 control the expression of a common set of genes. A. Gene-expression overlap determined by the microarray analysis of the transcriptome of RK3E^{TB} cells expressing shRNAs against Twist, Snail or Zeb1 (as in Smit & Peeper, 2011 Oncogene 30:3735-44). **B.** Common microarray outliers between RK3E^{TB} cells expressing two different shRNAs against Fra1 were overlaid with the 52 common Twist, Snail, Zeb1 targets identified as in A, revealing an overlap of 40 genes. **C.** Heatmap of the expression of the 40 genes commonly regulated upon silencing of Twist, Snail, Zeb1 or Fra-1.

Supplementary Figure 6. Fra-1 is commonly overexpressed in human breast cancer cell lines and is required for lung metastasis of breast cancer cells. A. Western-blot analysis of Fra-1 expression in human breast cancer cell lines. β-actin serves as loading control. **B.** Fluorescence imaging of the lungs of mice inoculated intravenously with 10^6 GFP-labeled

LM2 cells expressing a control or sh-Fra-1 vector as indicated, 35 days after inoculation. **C.** Quantification of the fluorescence in the lungs of mice described in B. (n=4 lungs, error bars: S.D. Asterisk, different from control with $P < 0.001$ based on a one-way ANOVA followed by PLSD test). **D.** Fluorescence imaging of the lungs of mice inoculated intravenously with 10^5 GFP-labeled LM2 cells expressing a control or sh-Fra-1 vector as indicated, 35 days after inoculation. **E.** Quantification of the fluorescence in the lungs of mice described in D. (n=4 lungs, error bars: S.D. Asterisk, different from control with $P < 0.001$ based on a one-way ANOVA followed by PLSD test). **F.** Images of the lungs (upper panel) and haematoxylin-eosin stained sections of the lungs (lower panel, scale bar: 100 μm; T: Tumor) of mice that were injected intravenously with 1.10^6 MDA-MB-231 cells expressing independent Fra-1 shRNAs as indicated, photographed at 3 months after inoculation. **G.** Macroscopic quantification of the lung metastases formed by MDA-MB-231 cells described in F (n=5, error bars: S.D. Asterisk, different from control clones with $P < 0.001$ based on a one-way ANOVA followed by PLSD test). Data are representative of two (B-G) or three independent experiments (A).

Supplementary Figure 7. Selective pressure for restoration of Fra-1 expression in pulmonary metastases formed by Fra-1-depleted cells. Immunohistochemical analysis of human Fra-1 or GFP expression in the lungs of mice inoculated by control or Fra-1-depleted LM2 cells, 114 days after inoculation of Fra-1-depleted cells (scale bar: 100 μm). As a control for the presence cells early after injection, staining of lung sections performed 90 minutes after inoculation of control and Fra-1-depleted cells is also shown. Data are representative of two independent experiments.

Supplementary Figure 8. Fra-1 is required for metastasis to multiple organs. A. Representative bioluminescence images of mice injected into the left cardiac ventricule with 10^5 MDA-MB-231 cells expressing a control or sh-Fra1 vector, as indicated, 49 days after cells inoculation. **B**. Quantification of the luminescence signal in the mice described in A. as a function of time (n=8-9, error bars: S.E. Asterisk, different from control for the two sh-Fra1 groups with * $P < 0.05$ or ** $P < 0.01$ based on a two-tailed Wilcoxon-signed rank test). **C.** Kaplan-Meier curves for survival of the mice described in A and B. Mice were euthanized when clinical symptoms became apparent (displayed P-value is based on a Log-Rank test). **D.** Haematoxylin-eosin staining of histological sections (M: metastasis) from control mice described in A and B (scale bar: 100 μm). **E.** Representative fluorescence imaging of the lungs of nude mice injected in the 4^{th} mammary fat pad with GFP-labeled LM2 cells expressing independent Fra-1 sh-RNAs, 6 weeks after surgical removal of the primary tumor. **F**. Quantification of the metastatic nodules in the lungs of mice described in E (n=10). **G**. Weight of the orthotopic LM2 tumors upon surgical removal after one month of growth, as a function of Fra-1 depletion (n=10, * P <0.001). Data are representative of two independent experiments.

Supplementary Figure 9. Fra-1 is required for EMT induced by MEK activation. A. Detection by immunofluorescence of E-cadherin (upper panel) and cytoskeletal actin (by phalloidin staining; lower panel) of control and Fra-1-silenced MDA-MB-231 cells. **B.** Western-blot analysis of E-Cadherin, Fra-1 and phospho-ERK levels in the human breast cancer cell lines LM2, MDA-MB-231 and ZR75-1, treated with the indicated concentrations of the MEK inhibitor UO126. ZR75-1 cells, which are negative for Fra-1 and positive for E-Cadherin are shown as negative controls. **C**. Western-blot analysis of E-Cadherin, Fra-1 and Phospho-ERK levels in LM2 cells stably transfected with an empty vector or a vector

encoding the stabilized Fra-1 mutant S252D/S265D (Basbous J. et al., 2007) treated with 10 μM of the MEK inhibitor UO126, as indicated. Panels in C were taken from a single blot. Data are representative of three independent experiments.

Supplementary Figure 10. A Fra-1-associated gene-expression profile accurately predicts clinical outcome of different breast cancer subtypes. Kaplan-Meier curves for signature-high samples and signature-low samples for time to distant metastasis (if available) or relapse on available breast cancer datasets. Patients were sorted based on their molecular subtype and stratified using the Fra-1 classifier. Also shown are the one-sided log-rank p-value and the Cox proportional hazards model hazard ratio between the signature-high and signature-low groups (see Methods).

Supplementary Figure 11. ADORA2B is expressed in ER-negative breast cancer and cells lines derived thereof. A. Expression levels of ADORA2B in the indicated breast cancer cell lines measured by quantitative RT-PCR (n=3, error bars: S.D.). The estrogen receptor status of the cell lines is also indicated. **B.** Expression levels of ADORA1, ADORA2A, ADORA2B and ADORA3 in the indicated breast epithelial or breast cancer cell lines measured by quantitative RT-PCR (n=3, error bars: S.D.). **C.** ADORA2B mRNA expression levels in the indicated breast cancer sub-groups obtained from the indicated datasets. Expression levels are different from triple-negative group with $P<10e^{-14}$ for $ER^{+}Her2^{-}$ group, $P=5.81e^{-8}$ for $ER^{+}Her2^{+}$ group, P=0.001 for $ER\text{-}Her2^{+}$ group, based on a random effects model (expression values from the different datasets were combined for each subgroup).

Supplementary Figure 12. ADORA2B expression is regulated by Fra-1 in human breast cancer cells. A. Expression levels of ADORA2B in the indicated breast cancer cell lines

measured by quantitative RT-PCR (n=3, error bars: S.D.) (left panel) and correlation between Fra-1 and ADORA2B mRNA expression (as determined in Figure S11*C*) in these cell lines (right panel). **B.** ADORA2B and Fra-1 expression levels in Fra-1-depleted MDA-MB-231 and LM2 cells, as indicated, measured by quantitative RT-PCR (n=3, error bars: S.D.). **C.** Schematic position of putative Fra-1 binding sites (numbered black arrows) identified in the promoter and first intron region of the *adora2b* gene (left panel) and relative enrichment for genomic DNA sequences spanning these individual sites in chromatin immunoprecipitation experiments using anti-Fra-1 or isotype control antibodies (right panel) (n=3, error bars: S.D.). Data are representative of three independent experiments.

Supplementary Figure 13. ADORA2B is required for breast cancer cells metastasis. A. ADORA2B expression levels in LM2 cells expressing 4 independent sh-RNAs targeting ADORA2B, as indicated, measured by quantitative RT-PCR (n=3, error bars: S.D.). **B.** Quantification of the fluorescence in the lungs of nude mice inoculated intravenously with 10^5 GFP-labeled LM2 cells expressing independent ADORA2B shRNAs as indicated, 35 days after inoculation (n=4 lungs, error bars: S.D. Asterisk, different from control with * $P < 0.05$ or ** $P < 0.005$ based on a one-way ANOVA followed by PLSD test). **C.** Fluorescence imaging of the lungs of mice described in C. **D.** Representative bioluminescence images of mice injected intravenously ($2x10^5$ cells) with LM2 cells expressing a control or sh-ADORA2B vector at different time points as indicated. **E.** *In vitro* proliferation curve of control and ADORA2B-silenced LM2 cells (n=3, error bars: S.D.). **F.** *In vivo* growth curve of tumors formed by control and ADORA2B-silenced LM2 cells injected in the 4^{th} mammary fat pad on both flanks (n=6 tumors, error bars: S.E.). Data are representative of two independent experiments.

Supplementary Figure 14. ADORA2B is not required for maintenance of EMT-like characteristics but is involved in migration and invasion of breast cancer cells. A. E-cadherin expression levels measured by western blotting in LM2 cells expressing a control vector, a sh-RNA targeting Fra-1 or independent sh-RNAs targeting ADORA2B as indicated. Actin serves as loading control. **B.** Phase contrast micrographs of LM2 cells expressing a control vector or independent sh-RNAs targeting ADORA2B as indicated (scale bar: 100 μm). **C.** Representative immunofluorescence imaging of the cytoskeleton of LM2 cells expressing a sh-ADORA2B construct or treated with 100 μM theophylline. Individual images of the staining of DNA with DAPI (upper panel), of α-tubulin (middle panel) and of F-actin (lower panel) are shown (scale bar: 10 μm). **D.** Invasion capacities of LM2 cells as a function of ADORA2B depletion or theophylline treatment (100 μM) (n=3, error bars: S.D. Asterisk, different from excipient-treated control cells with $P < 0.05$ based on a one-way ANOVA followed by PLSD test). **E.** Colony forming activity of LM2 cells in soft agar assays as a function of ADORA2B depletion or theophylline treatment (100 μM) (n=3, error bars: S.D. Asterisk, different from excipient-treated control cells with $P < 0.001$ based on a one-way ANOVA followed by PLSD test). Data are representative of 3 independent experiments.

Supplementary Figure 15. Theophylline can potentiate the cytotoxic effect of paclitaxel *in vitro*. Dose-response curves of LM2 cells treated with paclitaxel, either alone (DMSO) or in the presence of the indicated concentration of theophylline (n=4, error bars: S.D.). Values were normalized to untreated cells (without paclitaxel or theophylline). Data are representative of three independent experiments.

Supplementary Figure 16. Co-treatment of docetaxel and theophylline does not induce weight loss in mice. A. Representative bioluminescence images of mice injected

intravenously ($2x10^5$ cells) with LM2 cells and receiving the indicated treatment (docetaxel 4 mg/kg i.p. weekly and/or theophylline 10 mM in drinking water) at different time points as indicated (time points 7 and 14 days were excluded from the figure because bioluminescence signal was below the scale range). **B.** Weight curves as a function of time of mice injected intravenously ($2x10^5$ cells) with LM2 cells and receiving the indicated treatment (docetaxel 4 mg/kg i.p. weekly and/or theophylline 10 mM in drinking water). Values were normalized to the weight of the mice at the time of cell injection. Data are representative of two independent experiments.